PV System Information Enhancement and Better Control of Power Systems.

by

Syed Muhammad Yousaf Hashmy

A Thesis Presented in Partial Fulfillment
of the Requirement for the Degree
Master of Science

Approved September 2019 by the
Graduate Supervisory Committee:

Yang Weng, Chair
Arunabha Sen
Jiangchao Qin

ARIZONA STATE UNIVERSITY

December 2019

ABSTRACT

Due to the rapid penetration of solar power systems in residential areas, there has been a dramatic increase in bidirectional power flow. Such a phenomenon of bidirectional power flow creates a need to know where Photovoltaic (PV) systems are located, what their quantity is, and how much they generate. However, significant challenges exist for accurate solar panel detection, capacity quantification, and generation estimation by employing existing methods, because of the limited labeled ground truth and relatively poor performance for direct supervised learning. To mitigate these issue, this thesis revolutionizes key learning concepts to (1) largely increase the volume of training data set and expand the labelled data set by creating highly realistic solar panel images, (2) boost detection and quantification learning through physical knowledge and (3) greatly enhance the generation estimation capability by utilizing effective features and neighboring generation patterns. These techniques not only reshape the machine learning methods in the GIS domain but also provides a highly accurate solution to gain a better understanding of distribution networks with PV penetration. The numerical validation and performance evaluation establishes the high accuracy and scalability of the proposed methodologies on the existing solar power systems in the Southwest region of the United States of America. The distribution and transmission networks both have primitive control methodologies, but now is the high time to work out intelligent control schemes based on reinforcement learning and show that they can not only

perform well but also have the ability to adapt to the changing environments. This thesis proposes a sequence task-based learning method to create an agent that can learn to come up with the best action set that can overcome the issues of transient over-voltage.

ACKNOWLEDGMENTS

First, I would like to express my deepest gratitude to my advisor, Dr. Yang Weng, for offering great support on this thesis research. I sincerely thank him for his invaluable guidance, patience and encouragement throughout my master studies. He sets a good example of researcher to our group by his sharp engineering insight and great enthusiasm in research.

I would like to thank my committee members, Dr. Arunabha Sen and Dr. Jiangchao Qin for taking the time to give their invaluable feedback.

I would like to thank my supervisors Dr. Di Shi and Dr. Zhe Yu at GEIRINA, State Grid Corporation of China. Without their unwavering technical and moral support, while my stay at their organization as an intern, I would not have been able to make it in time. Lastly, I would like to thank my parents, Tausif Hashmy and Naeema Hashmy for their affection and support that stood by me, throughout my life.

TABLE OF CONTENTS

CHAPTER Page

LIST OF TABLES

Table Page

LIST OF FIGURES

Figure Page

Figure Page

Chapter 1

INTRODUCTION

United States has witnessed a dramatic growth in rooftop PV systems–around 50% every year, since 2012. The falling prices and the nature of clean and reliable power have been responsible for such a rapid growth [1]. Research estimates that 50 - 530 GW of solar-based power will potentially be available in the United States by the year 2040 [2]. The boom in modern ways of generating electricity has driven an enthusiasm in scientists and engineers alike to study PV systems in detail and asses the incoming challenges as well as out of the box solutions to the pressing problems, associated with them. The grid-connected solar power systems are expected to penetrate much rapidly into the picture than the off-grid ones [3]. The safety and stability of the system have to be ensured at all times, for that matter grid with PV integrations must meet the corresponding requirements of active power control, power quality, low voltage ride through, voltage regulation, frequency stability, system protection and load characteristics [4, 5, 6]. The generation of a solar power system is highly dependent on solar irradiance, terrain, weather, soiling and multiple other non-convex factors rendering the optimization problem a non-convex one [7]. Indeed, it is a far more difficult task to model such factors and deduce conclusions, with the currently available computational capa-

bility. This paper proposes a holistic approach to tackle this situation. Supervisory Control and Data Acquisition (SCADA) demands the research community to hunt for innovative solutions as is proposed by [8]. But, with the current outburst of uncertainties and variabilities in the distribution networks like renewable energy resources and demand response [9]. It is inevitable to channelize the investment of time and money to build up artificial intelligence (AI) based solutions, so that SCADA is well prepared to tackle the modern day challenges.

Ever since the distribution networks have faced a plethora of bidirectional generation at the secondary distribution level the necessity to locate them and predict their generations have been keenly explored. The interest lies in both long-term [10] as well as short-term [11] generation forecasting. [10] only considered the solar irradiation for a long period of time at a particular region and is unable to address the concern of limited features. [11] has introduced Support Vector Machine (SVM) as a base learner and meta learner of the Stacking algorithm, the K-means algorithm is used to cluster the training set for predicting the short term solar power generation. [12] details the performance of widely used machine learning techniques on weather data, irradiation, and geographical parameters and claims that Artificial Neural Networks should be preferred over Gaussian process, kernel ridge regression, boosted trees and regression trees. The generation of the past is also a key consideration while forecasting solar power generation. The accessibility to all such locations for gathering data is also a key to these studies. However,

we aim to identify the location of solar panels and predict the solar power generation for regions with limited accessibility.

Moreover, the topology of the distribution system is also gaining importance due to the active power generation at that level. The increasing penetration of distributed energy resources (DERs) posits several reliability issues. Topology estimation is also compromised [13]. The foreseeable future challenges due to the PV power-sharing [14] and its economics presents the challenge to have overwhelming access to the PV data and system topology. The PV generation data is scattered and there are several different sources, like solar panel manufacturers, inverter manufacturers, PV system development companies, utilities, and consumers. But, there are insufficient mechanisms in operation for data aggregation. The local data clouds not exhaustive. The paper provides a road map to combine publicly available cloud data with the validated local databases to achieve a more exhaustive database. Google Maps are one of the most widely used publicly accessible data [15]. But, the access is not utilized to its full potential for the rooftop solar power systems, that are scattered and abundant.

The boom in solar power system in recent past, gave rise to the pressing issues of the effects of renewable energy integration on the previously existing grid infrastructure. That may cause concerns related to situational awareness, planning, operations, and maintenance of the power system. The challenge can be addressed by a mechanism that can recover all the missing links in the knowledge

of the current power system. The inability to access certain data sources and the segregation of many independent cloud sources, are the responsible prime factors. The geospatial information of solar panels has been one of the victims of the underscored factors. To overcome such issues, the satellite images of solar power systems are a rich source and have been widely used for making predictions about places and events that are difficult to record by other means [16]. The feasibility of the fast, scalable and inexpensive scheme of detection of solar panels in satellite images is proposed in [16]. But, it fails to address the data deficiency issue. The rooftop solar panel detector tool is also discussed in [17], but it does not provide the details on achieving an estimate for PV generation.

A scheme is proposed in this paper that can help alleviate these issues of missing information. The privately available data is limited and it is possible to combine more than one source of data. But, this can not be achieved with rudimentary methods, as the growth in this domain has been explosive, but there is a need to develop robust methodologies that can help in fulfilling the need to a reasonable extent. This paper is focuses on systematic approach to connect the dots and provide thorough machine learning based solution.

Furthermore, the solar panels are mounted on the rooftops of the houses in large numbers. Many rooftop PV systems are also connected to the grid. The first part is the detection and localization of solar modules. Support Vector Machines (SVMs) are the popular machine learning techniques and have been widely used

for the classification and regression problems for various applications, including detection of PV systems as mentioned in [16]. The satellite images are subjected to SVM to capture the changes in PV generation due to moving clouds [18], builds up a strong contention in favor of applicability of SVM to problem set under discourse. The images are acquired from Google Earth in a specific ZIP Code area with dimensions 24×18 pixels. The methodology adopts a semi-supervised approach to detect, quantify and estimate the power generation capability. This paper combines the ideas together to solve a bigger problem. The operation and control of a distribution system rely heavily on the bidirectional power flow capability, hence the detection schemes need to be highly reliable, we propose a systematic mechanism for achieving accurate results. But, there exists the issues of deficiency of ground truth that needs to addressed first. Therefore, we propose to increase the data volume by numerous techniques. Methods such as flipping images have been popularly used. But we propose to gain more information by rotating slices. Such an approach helps in capturing the effect of different orientation angles of PV installations. In addition, the artificially created images with labels aid the learning process, as the model may not see all the possible cases in the real data, but artificially created data can provide such an insight. For example, it is possible that images with 5 solar panels may never appear in training data, then we can artificially create such labelled instances and add them to boost the training process.

Along with a good training data, we need a robust detection algorithm, there-

fore we carefully design the detection model that takes advantage of prominent characteristics related to chromatic, geometric and relative relationship of the solar modules. Such an approach enables the model to produce robust and highly accurate detection results. Once the location of PV system is determined accurately, we need to know its quantity. While quantifying the modules, we provide the quantization approach instead of the area covered to overcome the approximation errors and get high accuracy.

Knowing the quantity has its advantage of gaining insight into the generation capability, but its effectiveness can be enhanced by having the real time PV generation profile. So to estimate generation, we consider the effect that the PV generation patterns of neighboring houses are similar, because of their exposure to similar sunshine. Therefore, we propose to utilize the generations from the nearest neighbors. But such an information alone can add a bias and may not deliver the accurate generation profile. Therefore, we add relevant features for improving the information gain, like the geographical position and altitude for measuring "closeness" and temperature due to its high correlation with PV generation. Hence, we conduct nearest neighbor approach based on weighted estimation. The performance of the proposed method shown in Fig. 1.1, is verified by simulations on the SunPower Inc. data for 200 distinct locations from two different states namely, Arizona and California. The images are acquired from Google Earth. All simulations are conducted via Python. The results indicate that the method is highly accurate

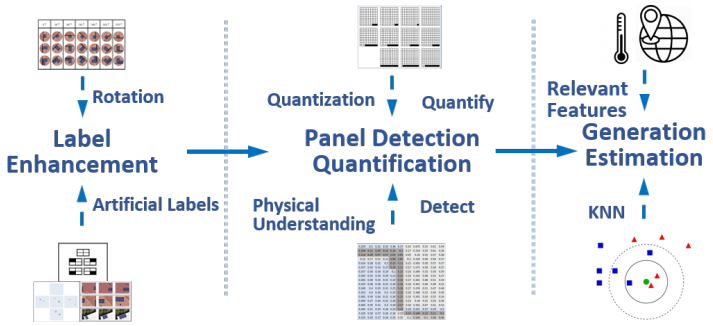

Figure 1.1: Scheme Proposed Technique.

and outperforms the previous methods.

Moving on to the control of the distribution grid, due to increase in the development of urban areas overhead distribution system control has been very significant. Also, the advancements in the manufacturing of cross-linked polythene (XLPE) extruded insulation technology has increased the use of Extra High Voltage (EHV) underground cables. In certain areas a combination of both overhead and underground cables is used and are typically referred to as hybrid circuits or mixed circuits. As a result of transient nature of faults on overhead transmission lines, auto-reclosing is the preferred method among Utilities. However, reclosing isnt recommended for underground cables as faults are permanent and can cause significant damage to the cables. In extra high voltage applications, metal oxide surge arresters and breaker with closing resistors are two basic methods to restrict switching surges [3]. In high voltage transmission systems, switching surges are destructive to electrical equipment, so surge arresters are typically installed near large transformers and online terminals to suppress surges [5]. Whereas in

medium and low voltage levels, as the penetration of distributed energy resources gets deeper, it is still not clear whether the arresters are a viable solution.

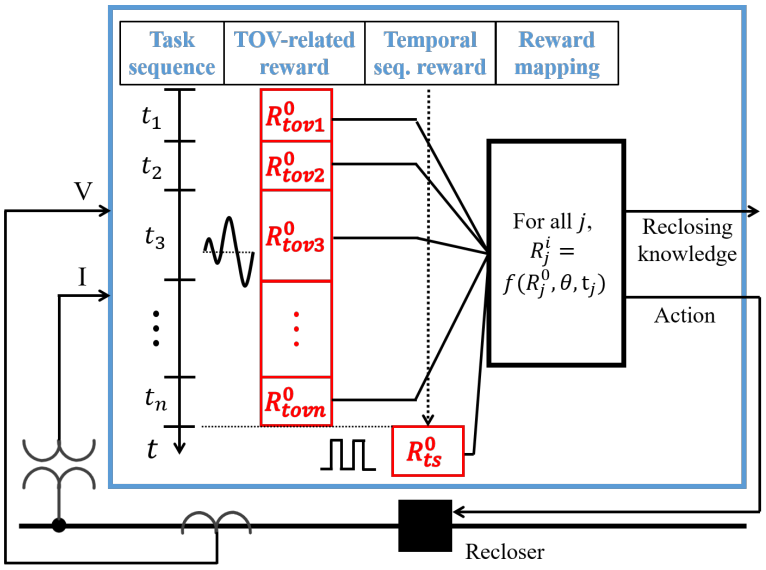

Figure 1.2: The Temporal Sequence Reward Mechanism For TOV Mitigation.

Chapter 2

MODELLING

In this section, we first describe the Google Earth solar panel images as given vectors. Such a definition enables us to process the PV panel images and formally define the problem of solar panel detection in images and their respective generation prediction. Here, the raw solar panel images are $\boldsymbol{x}^{raw} \in \mathbb{R}^p$, where p is indicative of the dimensions of PV panel image. The images are segmented into 100 smaller images and also flattened to get x_i^p, where $p = 1, \cdots, P$ is the dimension of each vector and $i = 1, \cdots, N$ is the number of samples (images). The existence of solar panels is depicted by the label $C_i \in \{1, -1\}$, where 1 shows the existence and -1 shows non-existence. The quantity q_i gives the count of solar modules in the solar panel image. Moreover, y_t, where $t = 1, \cdots, T$ time points, is the generation prediction of the corresponding solar power system, given the generation g_t^k, $t = 1, \cdots, T$ of k nearest neighbors.

2.0.1 Problem Definition

The problem is defined as follows.

- Problem: location detection, quantity assessment and power generation estimation of rooftop solar power systems.

- Given:

    1. raw image $\boldsymbol{x}^{raw}$ from Google Earth,

    2. known PV generation time series g_t^k of solar panel systems covered in the $\boldsymbol{x}^{raw}$ solar panel image.

- Find: for a single segment x_i^p image of solar panel,

    1. existence C_i of solar panels,

    2. quantity q_i of solar modules,

    3. power generation time series y_t prediction.

Chapter 3

PV DETECTION AND GENREATION ESTIMATION

3.0.1 Detection Methodology

SVMs are supervised machine learning methods that were originally developed for classification but they can also be used for regression by maximizing the distance between the decision boundary and the closest training sample for finding the optimum decision boundary. The margin describes shortest distance between the decision boundary and the closest data element, so, SVM can also be called as maximum margin classifier [19]. Each training sample is segmented and flattened PV image vector x_i^p, $i = 1, \cdots, N$ and $p = 1, \cdots, P$. Let us assume an adjustable solar panel vector of weights ω, which is the depiction of the slope of hyperplane at each point in the feature space and a bias term b representing the intercept of the hyperplane. Then, the optimization problem for linearly separable cases can be depicted as

$$\min_{\omega,b} \frac{1}{2}\omega^T\omega, \tag{3.1}$$

subject to

$$C_i(\omega^T x_i^p + b) \geq 1. \tag{3.2}$$

The above constraint enforces the hyperplane to distribute the samples into two linearly separable groups. But, the PV image data are not linearly separable.

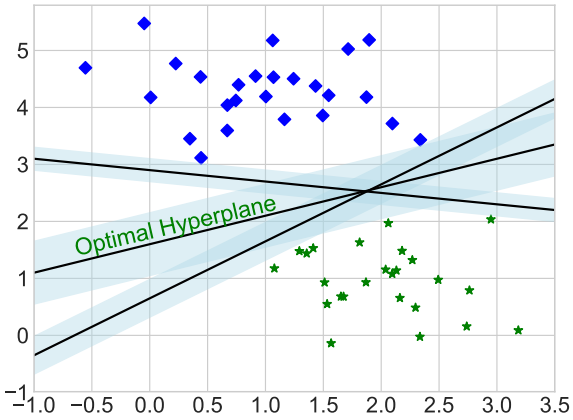

Figure 3.1: Decision Boundary of SVM.

Since, there are several different technologies available in market, e.g., Thin-Film, Mono-Crystalline and Poly-Crystalline Silicon panels. Moreover, the inclination and orientation angles are subject to the geography. So, a slack variable ς_i is introduced for each solar panel image to minimize the classification error. So, the updated primal optimization problem is

$$\min_{\omega,b,\varsigma} \frac{1}{2}\omega^T\omega + \gamma \sum_{i=1}^{n} \varsigma_i, \tag{3.3}$$

subject to

$$C_i(\omega^T x_i^p + b) \geq 1 - \varsigma_i, \tag{3.4}$$

$$\varsigma_i \geq 0, \tag{3.5}$$

γ is a scaling factor, controlling the weight between complexity of the machine and the number of non-separable points. Using Lagrange multipliers method with the Kuhn-Tucker conditions [20], we may formulate the dual problem for non-

Figure 3.2: Real Image Slices.

separable patterns. A kernel function help SVMs to solve the non-linear classification problem. The input space of solar panel image vectors is transformed by ϕ into a feature space of a higher dimension, where it is easier to find a separating hyperplane [21]. So, the inner product of $\phi(x_i^p)$ and $\phi(x_j^p)$ gives the kernel

$$K(x_i^p, x_j^p) = \phi(x_i^p)^T \phi(x_j^p). \tag{3.6}$$

The polynomial kernel function with degree 3 is widely used in power system applications.

$$K(x_i, x_j) = (x_i \cdot x_j + 1)^3. \tag{3.7}$$

Thus, the kernel can side-step the problem of data being non-linearly separable by implicitly mapping them into a feature space, where a linear threshold can be used directly. Using a kernel is equivalent to solving a linear SVM in some new higher-dimensional feature space [21]. Therefore, a non-linear SVM score is

a linear combination, but with new variables, which are derived through a kernel transformation of the solar PV images x_i^p.

The dual has linear constraints, which implicates that the problem solution becomes convenient. Hence, for the primal in expression 3.3 can be converted to its dual, where λ_i, $i = 1, \cdots, N$ is the Langrange multipliers

$$\min_{\lambda} \frac{1}{2} \sum_{i=1}^{N} \sum_{j=1}^{N} \lambda_i \lambda_j C_i C_j K(x_i^p, x_j^p) - \sum_{i=1}^{N} \lambda_i, \tag{3.8}$$

subject to

$$\lambda_i C_i = 0, \tag{3.9}$$

$$0 \leq \lambda_i \leq \gamma, \tag{3.10}$$

where, $i = 1, \cdots, n$ is the formulation for evaluating optimal Langrange multipliers. The decision function for test images x_{test}^p is

$$sgn(\sum_{i=1}^{N} C_i \lambda_i K(x_{test}^p, x^p) + b). \tag{3.11}$$

3.0.2 Quantification Methodology

Support Vector Regression (SVR) is widely applied for the regression problems, as discussed indepth in [22]. By using a mapping, $\Phi : X \rightarrow F$, where X is the domain and F is a high-dimensional feature space. SVR approximates unknown functions in an output space Y, while operating in feature space F. Thereby using nonlinear functions to linearly estimate an unknown regression [23]. In a nutshell, SVR models a way to generalize the inputs in accordance with the training image dataset x_i^p, where $i = 1, \cdots, N$ image samples and $p = 1, \cdots, P$ is the dimension of

each image vector. The solar panel count q_i, $i = 1, \cdots, N$, is to be determined. Unlike SVC, SVR has two different slack variables, one for upper decision boundary and another one for lower decision boundary. Hence, ς_i^* is also introduced and the optimization problem becomes

$$\min_{\omega,b,\varsigma,\varsigma^*} \frac{1}{2}\omega^T\omega + \gamma \sum_{i=1}^{n}(\varsigma_i + \varsigma_i^*), \tag{3.12}$$

subject to

$$C_i - \omega^T x_i^p - b \leq \epsilon + \varsigma_i, \tag{3.13}$$

$$\omega^T x_i^p + b - y_i \leq \epsilon + \varsigma_i^*, \tag{3.14}$$

$$\varsigma_i \geq 0 \tag{3.15}$$

$$\varsigma_i^* \geq 0, \tag{3.16}$$

where ϵ is a hyperparameter that gives a margin of tolerance. The higher its value is, the larger is the allowable error, thus helps controlling the complexity of the model. Similarly, a kernel matrix K is used, and with that the computational complexity of the model is reduced because the actual high-dimensional mapping is not there anymore. For making the solution more convenient, the dual is used and a new Langrange multipliers λ_i^* is also introduced in [23].

$$\min_{\lambda} \sum_{i=1}^{N}\sum_{j=1}^{N} \lambda_i\lambda_j K(x_i^p, x_j^p) - \sum_{i}^{N} q_i + \sum_{i=1}^{N} |\lambda_i|\epsilon, \tag{3.17}$$

subject to

$$\sum_{i}^{N} \lambda_i = 0, \tag{3.18}$$

$$\lambda_i \geq -\gamma, \tag{3.19}$$

$$\lambda_i^* \leq \gamma, \tag{3.20}$$

where $i = 1, \cdots, N$. The polynomial kernel function of degree 3 can be applicable here as well. The final decision for test images x_i^p, $i = 1, \cdots, N$ and $p = 1, \cdots, P$ is

$$q_i^* = \sum_{i=1}^{N} (\lambda_i - \lambda_i^*) K(x_i^p, x^p) + b. \tag{3.21}$$

Since, $q_i^* \in \mathbb{R}$ and have non integral values, but the problem set should have quantified integral values. The solar panel count can only be a positive real integral value. So, the floating point samples should first be discretized into the algebraic-integer representation [24],

$$q_i = nearest\ integer(q_i^*). \tag{3.22}$$

3.0.3 Power Generation Estimation Methodology

The Euclidean distance is a promising measure for the distance between any two samples in a feature space. It is described in detail along with some other distance metrics in [25]. The coordinates of PV system location are well known, because the location has been identified. Let q_i, $x_i^{latitude}$ and $x_i^{longitude}$, $i = 1, \cdots, N$, form the features of $\boldsymbol{S}_i \in \mathbb{R}^3$. Now, the distances of a new test sample $\boldsymbol{S}_{test} \in \mathbb{R}^3$ comprising of three features q_{test}, $S_{test}^{latitude}$ and $S_{test}^{longitude}$ with k number of training samples can be calculated in Euclidean manner.

$$d^k(\mathbf{S}_k, \mathbf{S}_{test}) = \sqrt{\sum_{f=1}^{3} (S_k^f - S_{test}^f)^2}, \tag{3.23}$$

where $k = 1 \cdots, K$ and d^k is the vector of distances. In the feature space, the closest K points to $\boldsymbol{S}_{test}$ are used for the training purposes. Their respective distances are used as the weights d_k and the PV generation time series of k nearest neighbors are represented as g_t^k. For $t = 1, \cdots, T$ time points, the PV generation of the unknown solar power system is given by y_t. The optimization problem becomes

$$\min_{d,g} \sum_{i=1}^{N} \sum_{k=1}^{K} \sum_{t=1}^{T} |y_t - d^k g_t^k|^2. \tag{3.24}$$

This procedure gives an estimate of power generation for the unknown rooftop solar power system. The proposed procedure is elaborated in the algorithm.

Chapter 4

DATA ENHANCEMENT

The data source for images is always limited as compared to the volume of scenarios that exist in the real world. The performance of machine learning models is affected by the size of the training set [26]. So, we came up with a methodology to increase the size of the training dataset, in order for the machine learning model to achieve better performance. We propose that the images should be cropped first in a circular fashion since the traditional approach of using rectangular images would lose information upon rotating about a fixed axis as proposed in [27] and [28]. For example, the information around edges and vertices will be compromised, and the performance will suffer. Circular segmentation based approach is touted in [29], which is invariant of rotation and can show promise in reliable data generation.

Furthermore, an in-depth analysis is carried out to illustrate the effect of rotation of the image. Since Google Earth images may have any possible orientation, but all of them might not appear in the training scenarios. Hence, a rotation scheme is developed to enable the model to perform well in scenarios with newly created orientations, as well. Several image rotation techniques are proposed in literature [30]. The training images are rotated by 45°, 90°, 135°, 180°, 235° and 270°. The intention to retain as much information as possible leads to the approach of the

circular crop. It helps in having complete control over the rotation without losing any information. The images are fed to the model and testing results are recorded. The results show, that the number of solar panels in the rotated images are determined with reasonable accuracy by the proposed model of SVR. The rotated images are shown in Fig. 4.1.

Taking a case of image with vectors $P = P_1, P_2, P_3, \cdots, P_n$

$$l^2(O, P) = ||P||^2 = \sum_{i=1}^{n} p_r^2. \tag{4.1}$$

The similar result can also be obtained by the inner product of the two vectors,

$$||P||^2 = \begin{pmatrix} p_1, p_2, \cdots, p_n \end{pmatrix} \begin{pmatrix} p_1 \\ p_2 \\ p_3 \\ \vdots \\ p_n \end{pmatrix} = P^T P. \tag{4.2}$$

The distances or the ratios among the distances remain the same while the points are transformed about the center. From these properties it can be shown that a rotation is a linear transformation of the vectors, and thus can be written in matrix form QP. So, the equation 4.2

$$P^T P = (QP)^T QP, \tag{4.3}$$

$$P^T P = P^T Q^T QP. \tag{4.4}$$

If I is the identity matrix, then

$$P^T I P = P^T (Q^T Q) P. \tag{4.5}$$

Hence, the rotation matrix should fulfil the first condition

$$Q Q^T = I, \tag{4.6}$$

and it should preserve the handedness, i.e., the determinant of the matrix should be unity, which is the second condition

$$\det(Q) = 1. \tag{4.7}$$

If both the conditions are satisfied, then Q is regarded as a rotation matrix, thus the rotated raw image will be

$$\boldsymbol{x}_i^{raw,rotated} = Q\, \boldsymbol{x}_i^{raw}, \tag{4.8}$$

where $i = 1, \cdots, N$.

The numerical validation of the algorithm is discussed in the following section.

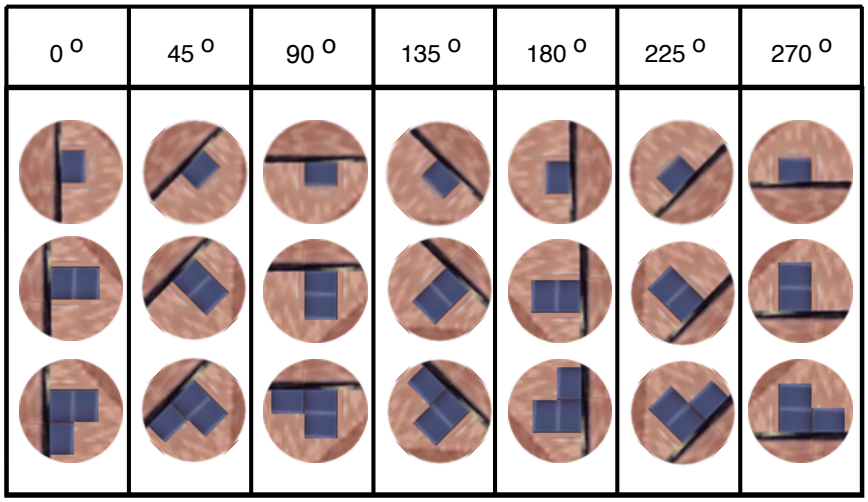

Figure 4.1: Data Generation Through Rotation.

Chapter 5

NUMERICAL VALIDATION

5.1 Data Preparation

The publicly available image dataset of PV systems is available in abundance, in the form of Google Earth. The images are acquired by fixing altitude to $900ft$ and elevation angle to $0°$. The images might either be of Joint Photographic Experts Group (JPEG) or Portable Network Graphics (PNG) format, both are similarly processed. The size of the image is kept 24×18 pixels because each large image is sliced into 100 small images as shown in Fig. 3.2. These images are sliced through an image slicer package of python.

5.2 Why Support Vector Machine Works While Others Do Not

For the current application, an algorithm based on Support Vector Machine (SVM) is developed on Python framework for the detection of solar panels. It has an established upper hand over other techniques. The data particular to solar power systems is scarce, and that is one of the fundamental problems we are trying to address in this paper. The deep learning based algorithms were also developed to locate and quantify the solar panels in the images, but could not achieve convincing results, as supported by [31] Convolutional Neural Networks (CNNs)

have limitations when it comes to the real settings and scarce data. The over-Fitting is another major concern. [31] also proves a point about performance degradation of CNNs when subjected to real world images of average visual quality. As the satellite images are of varying qualities, SVM based regression has a upper hand over Neural Networks die to the limited amount of accessible data. SVMs deliver a unique solution because the optimization problem is convex. Whereas, Neural Networks, have multiple solutions associated with local minima and for this reason may not be a robust for such a problem. Another important aspect is the kernel, which can help in the detection of the depth of the image well, whereas the CNNs lack in identifying it unless there is a very large amount of training data.

Naive Bayes is another popular classifier, but it has a very strong assumption of independently identically distributed features, which is a rare case in realistic datasets similarly indicated in [32]. The random forest algorithm has a drawback of uninterpretability due to the apriori choice of the number of trees and randomization predominance in the decision [33], which is not as effective in case of SVM.

5.3 Systematic Approach of PV Detection and Quantification

SVC is implemented to assign the label to each image on the basis of the presence of a rectangular black block, which is used to show the solar panel presence in the image. But, in order to reach that result, first, the toy examples are created to make the problem simpler and gradually increasing the complexity and reaching close to the ultimate goal, step by step. Hence, software like Microsoft Paint and

Powerpoint are used to create such toy images. The image sizes are kept suitable for the model input and the image matrices are developed to loosely match the real images to be fed to the recognition algorithm. The images have different patterns and the changes in the patterns are deliberately made so that the performance of the image recognition algorithm is exploited to its maximum. The images are vectorized as proposed by [34].

At first, the image having size 2×2 are converted to vectors that are used for training and testing. The images have four blocks in total, that are arranged in two rows and two columns without leaving any space between them. Upon satisfactory image recognition results, the rows and columns are increased to 10 each, then to 100 each and finally adding some random noise to the images. SVM is put to trial and tuned to get the accurate results.

The black and white grid of the size 2×2 are formed and one of the four blocks is colored black, while the other ones are colored white. Whereas one of the images has all four blocks, white. Thus, there are five images that are depicted in Fig. **??**. SVC is used to identify whether there is a black block in the image. The model has detected the presence of a black block with 100% accuracy. Hence, it was established that the model was successful in classifying the specific image, that does not have any black block, building the argument on that, further larger and more complex images are trialed through the proposed model. The evaluation of the method was then scaled up to 3×3 grid created by following a similar procedure,

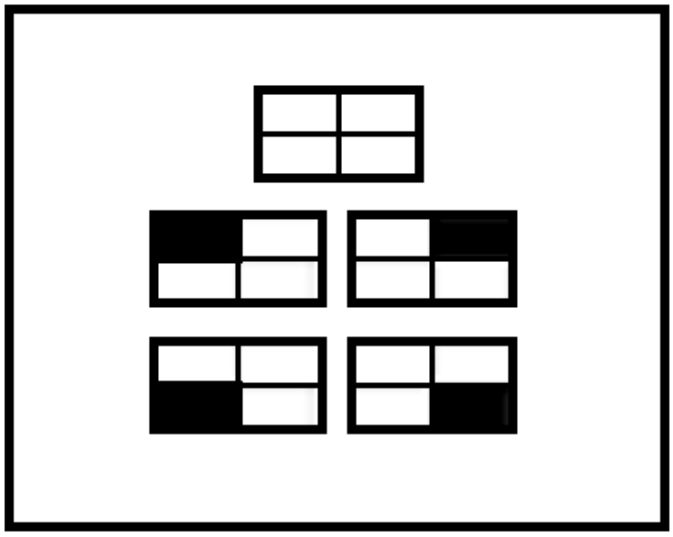

Figure 5.1: Five Images.

i.e., the images are having nine blocks and each image has one black block except one, which does not have any dark block. There are nine possible cases of having a single black block, Figure 5.2 shows all ten images. SVC was trained on the data set. The testing images are also vectorized and the predictions are monitored carefully, for all cases. The image classification method has once again established its effectiveness with 100% accuracy.

5.4 Black And White Images With Hundred Blocks

The case is extended further for as large as 100 blocks (10 rows and 10 columns). One of the blocks is darkened in each of the images. The dark blocks were picked up randomly. The images were passed through the same process of SVC. The result was once again, an encouraging one. That brings the methodology one step closer to recognizing the original solar panel representation in real images.

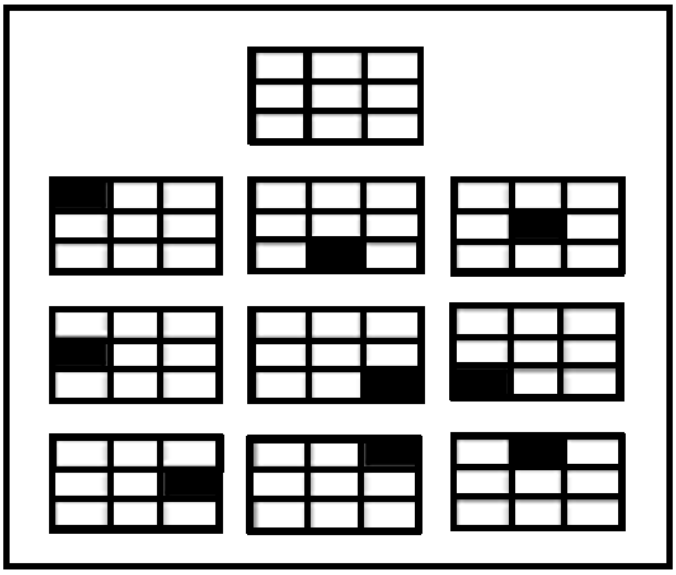

Figure 5.2: Ten Images.

5.5 Black And White Images With Thousand Blocks

The problem set is then extended to a grid of 100×100, rendering the images to be of 10000 blocks, 1 out of 10000 blocks is darkened. The similar procedure is reiterated on 10 images, having a dark block at different locations. The images are then fed to the SVC model to evaluate whether it is recognized or not. The model is perfectly able to recognize the existence of the dark block in this case.

The same 100×100 grid images are converted to blue lines and the blocks are 100×100 having shapes similar to those of the solar panels (11×5), i.e., blue with outliers modeled as green colored randomly sized objects. The rectangular block is precisely cut to have consistent dimensions for all the images. The images are then fed to the SVC model for the training. They were being tested one by one. The result of the test was accurate.

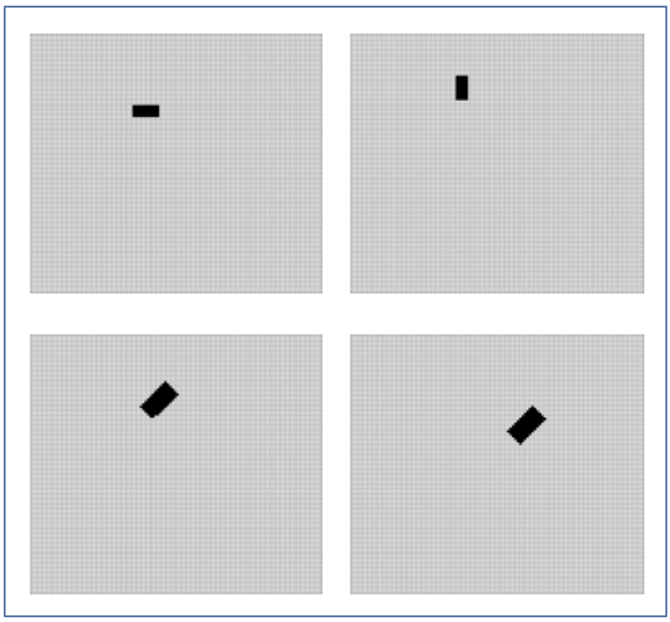

Figure 5.3: Four Images.

Figure 5.4: Five Images With Noise

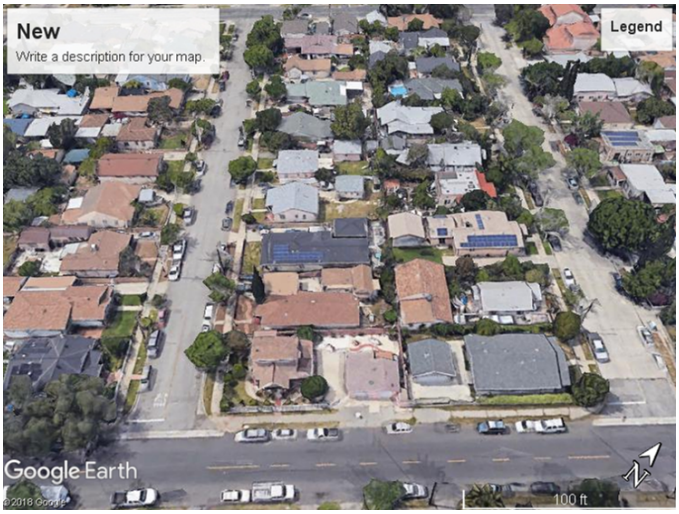

Figure 5.5: Real Colored Images.

5.6 Colored Images With Five Hundred And Four Pixels

All the results obtained in the above sections streamline the process of recognition of real satellite images acquired from Google Earth, the image recognition of the solar panels with some outliers should be working and on that assumption. The next step is to take the real satellite images centered at particular coordinates in the private database. The location is known to have solar panels. The satellite image is stored as JPEG format. The real image is centered at one of the coordinates from the privately available data. The source of the privately available cloud is SunPower Inc.

The images are cut into 100 smaller images each with 102×76 pixels. Hence, some images had the solar panels and most of them did not have any solar panels in them. The images were collated into a test data format by vectorizing every

image and manually labeling it with 0 (indicating the absence of solar panels) and 1 (indicating the presence of a solar panel). The images are vectorized by shifting all the columns, resulting in one row, without losing any element. So, all the vectors are 2356 elements long. It is subjected to the same SVC model. The model is trained on the images of the same sort. Some of the solar panel images are kept out of the training set and are later used for testing. The model is able to detect the presence of solar panels. The result is accurate. The testing is repeated several times by putting other images in the testing set that were initially present in the training set alone.

As the solar panel detection has been successfully achieved. Unfolding the whole procedure depicts that the model is capable of identifying the presence of a solar panel in the satellite image. An accuracy of 90.72% is obtained with the satellite images, that is better than the accuracy achieved by [35]. The results have been bolstered by the semi-supervised approach, by proving it true for the 100×100 blue colored grid with some green outliers. Zooming in and detecting a single black block in 100×100 grid. As 10×10, 3×3 and 2×2 grid is already considered and a single black block is accurately detected.

5.7 Quantification Of Solar Panels In Satellite Images

The presence of solar panels in an image has been identified with a very high accuracy using the proposed model. The next step is to develop a technique to predict the quantity of the solar panels in the image so that the generation estimation

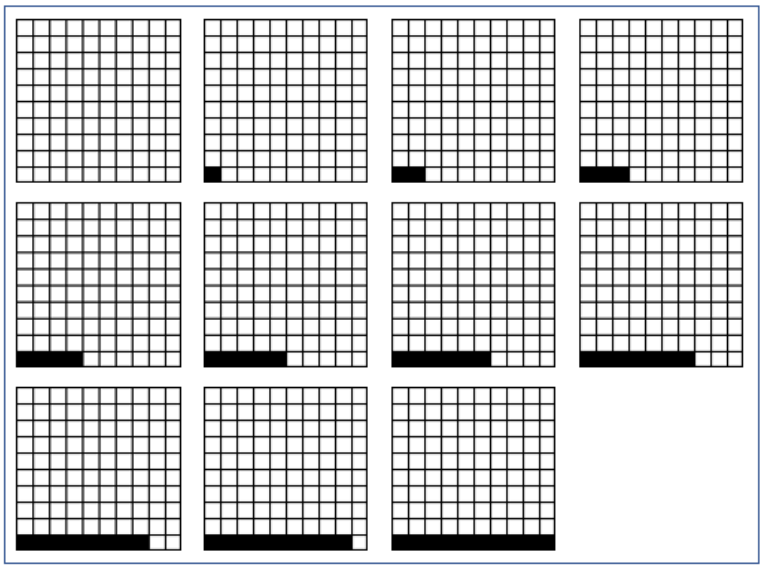

Figure 5.6: Elecven Images.

can be made with reasonable accuracy. The Support Vector Regression (SVR) is applied for solving the problem. Again, the training and testing images are converted into vectors for further processing.

5.8 Image With Hundred Blocks

The images with a grid of 10×10 blocks were created and then the incremental number of blocks were colored black and then the number of black blocks was used as the labels, shown in Fig. 5.7. The images were then fed to the SVR. The hyperparameters were kept at the default value. At first, the kernel was Polynomial Function, the degree is chosen to be 3. The result was obtained with reasonable accuracy.

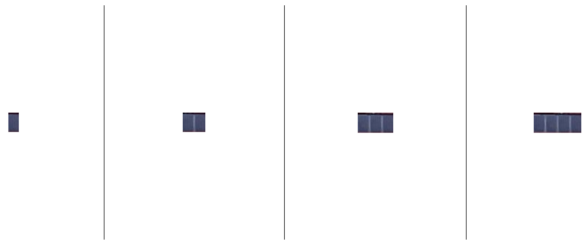

Figure 5.7: Panels On White Background.

5.9 Images With Varying Backgrounds

The real images of solar panels were projected on a white background. Those images were created with an increasing number of solar panels. The images were vectorized and then labels were assigned on the basis of the number of solar panels, visually recognized in the images. The images are then fed to the SVR model.

Table 5.1: Percentage Accuracies.

Performance Metrics	Accuracy Without Data Processing (%)	Accuracy With Data Processing (%)
Solar Panels Present	73.23	90.72
Solar Panels Absent	81.56	96.11

All the images have a white background. The solar panels are cropped and

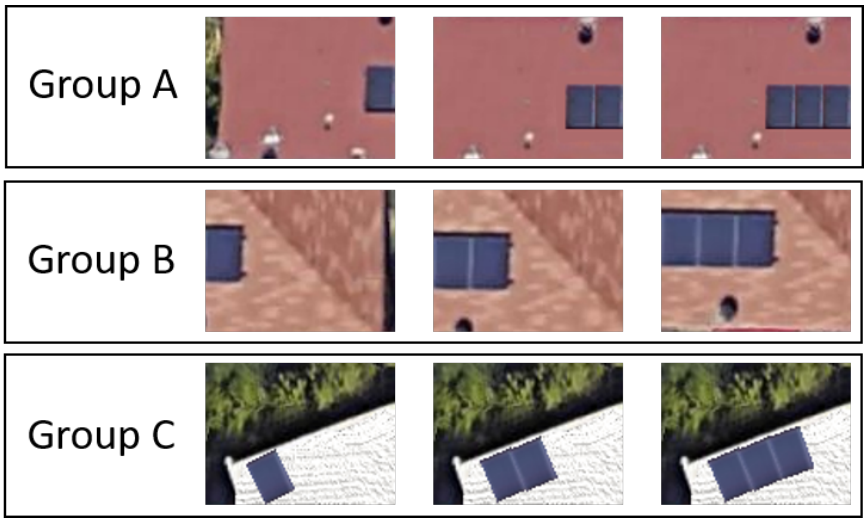

Figure 5.8: Real Images From Google Earth.

placed on top of the white background. Five such images are created. However, all five have a different number of solar panels in them, starting from one to five. The labels are assigned to the vectors of the images respectively. The images are subjected to SVR. The number of solar panels in the image present in testing is to be predicted by the model. The images with one solar panel and five solar panels are estimated with relatively higher percentage error. Whereas, the other ones are predicted with high accuracy. For every prediction, only the image to be predicted is not present in the training set, while the rest of the images are kept in the testing set. Polynomial kernel of degree 3 is used for SVR. Tolerance and epsilon are kept at very small values of 0.001 and 0.0001, respectively.

Images with three different types of backgrounds are used as the training and testing dataset, for the further experimentation. The images are processed beforehand by cropping the solar panels placing them over different backgrounds, in dif-

ferent numbers. The number of solar panels in the presence of real backgrounds are predicted by SVR again. The results show that, there exists an error between the real and predicted values of the number of solar panels when the backgrounds change dramatically. The testing is performed for the maximum of 5 number of solar panels, because the full exposure of maximum number of 5 solar panels in the specified zoom level.

The images supplied by Google Earth have several benefits over its rival Geographic Information Systems (GIS). [36] proves the high resolution imagery archive have robust positional accuracy. The horizontal and vertical positional accuracies play a vital role when it comes to solar panel image classification and quantification. In addition, the methodology focuses on a GIS, that is essentially open source like Google Earth, so that the overheads are limited.

5.10 Effects Of Hyper-parameters

The results are tested for different hyper-parameters, in order to have the best output of the SVR model. The relationship of the degree of the polynomial is studied. By varying the values of the degree from 1 to 8, the results indicate that 2^{nd} and 3^{rd} orders have been delivering the best results. Moreover, the effect of the coefficient is also studied, by using different values such as 0, 0.01, 1 and 10. The outcome indicates that there is no effect of the coefficient on the problem set under discussion. The hyper-parameter tuning package named GridSearchCV is used for further analysis. Its results are validated by comparison with the real scenarios.

The proposed technique is then evaluated for different case studies and the performance is elaborated in the next section.

Chapter 6

PERFORMANCE

The location of solar panels and the number of solar panels are predicted with reasonable accuracy. Both of them, are used as the features for the detection of power generation of the solar panels. The visualization of the generation characteristics in Fig. 8.1 shows a clear correlation among the neighboring PV systems. Therefore, the nearest neighbor approach is used to determine the solar power generation of the solar panels that are unknown. The areas under consideration are from two different states of the United States of America, 1) Tempe, Arizona and 2) Santa Ana, California. They differ in solar irradiance, climate, soiling profile and terrain from one another [37]. The generation of such solar panels is provided by SunPower Inc., and is is used as the training set for learning. K-Nearest Neighbor (KNN) method is used for assigning the weights to the time series of the nearest points on the map.

The time series of the generation for the past three years is used for the training. The inputs include the coordinates and the count of solar panels. The prediction of generation for the test case is compared with the original time series. 1 to 6 nearest neighbors are considered for simulation. The mean square errors (MSE) and mean absolute percentage errors are shown in . MSE is calculated using the

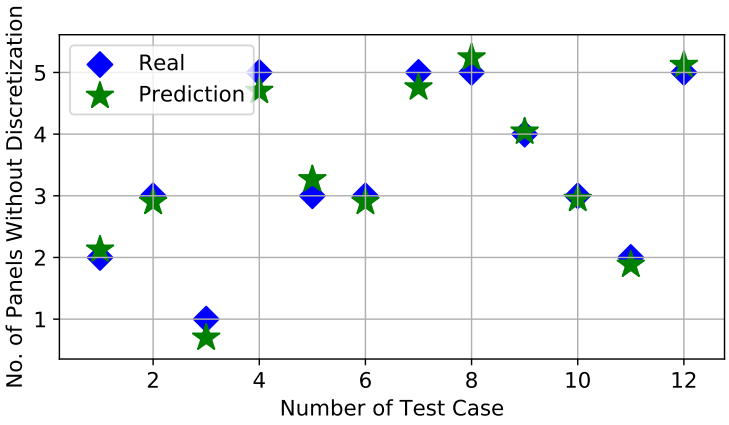

Figure 6.1: Prediction and Real Number Of Solar Panels Without Discretization.

predicted power generation time series y_t and real power generation $y_{t,real}$, where $t = 1, \cdots, T$ are the time points

$$MSE = \frac{1}{T}\sum_{t=1}^{T}(y_{t,real} - y_t)^2. \tag{6.1}$$

The variance of the distribution can be captured well in mean absolute percentage error (MAPE)

$$MAPE = \frac{1}{T}\sum_{t=1}^{T}\frac{(y_{t,real} - y_t)}{y_{t,real}} \times 100\%. \tag{6.2}$$

The annual generation of rooftop solar power systems show that over the long duration of time, neighboring generating units, have the similar trend. The solar power systems have the similar trends of the peak power generations, if they are located in the neighboring regions.

The results in Fig. 6.5 clearly show the fact, that 3 is the optimal value of k. If k is either smaller or larger than 3 the error increases. If it is increased further from 3, the distance keeps on building up the error. If it is lower than 3, than the bias

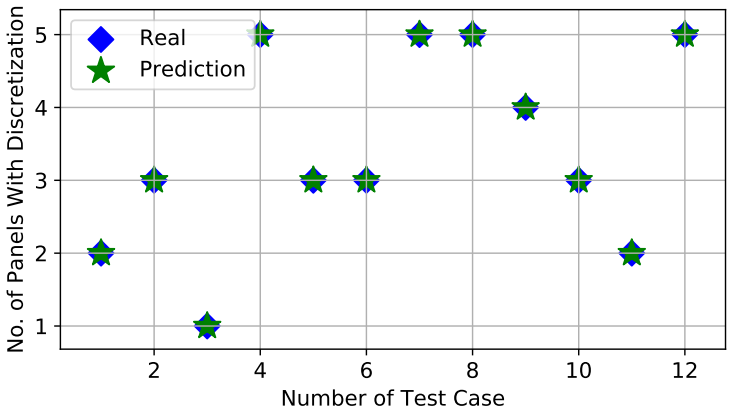

Figure 6.2: Prediction and Real Number Of Solar Panels With Discretization.

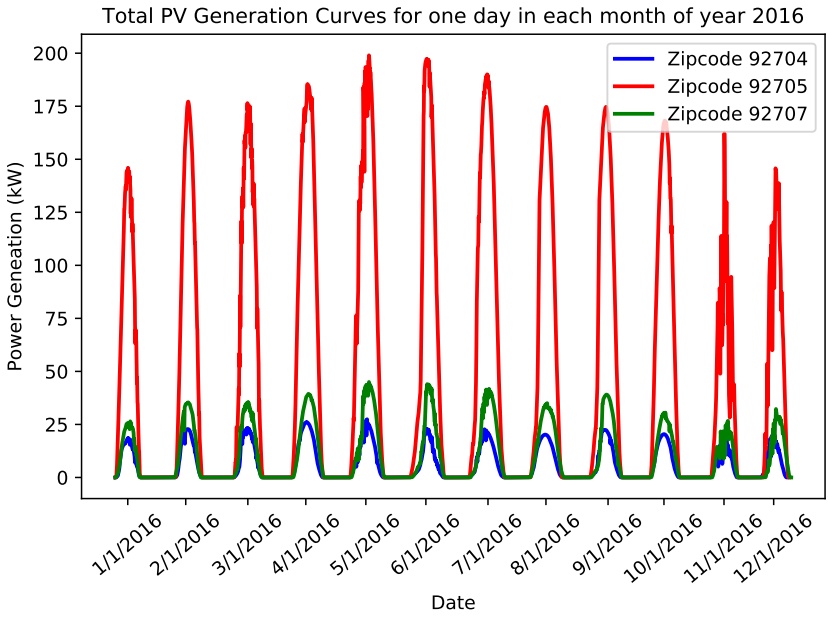

Figure 6.3: Peaks Of The Sum Of Solar Power Generation.

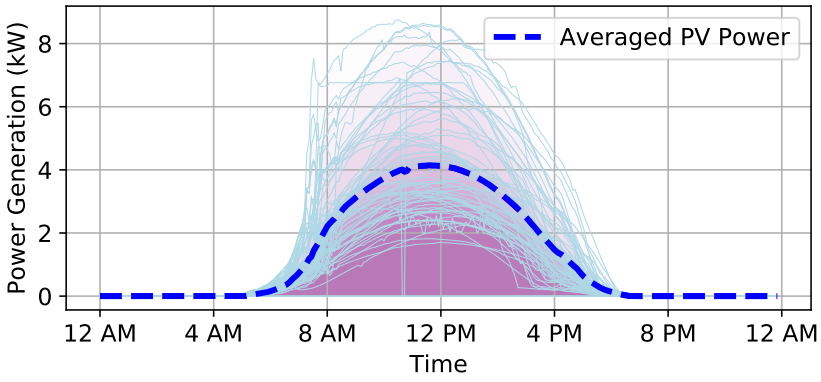

Figure 6.4: Raw data From SunPower Inc.

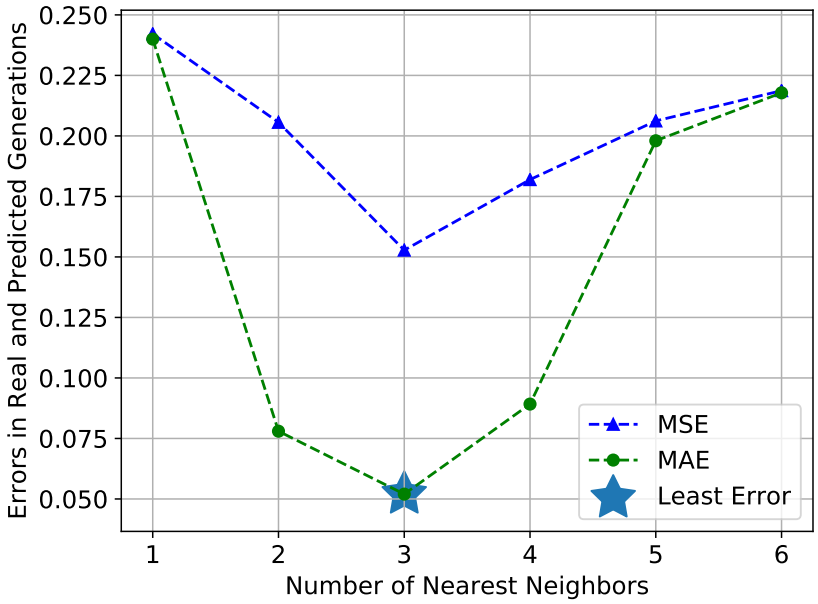

Figure 6.5: Nearest Neighbors.

Table 6.1: MSE And MAPE Of Real And Predicted Generations.

No. of Neighbors	MSE	MAPE (%)
1	0.2422	24.14
2	0.2056	7.80
3	0.1528	5.21
4	0.1819	8.92
5	0.2062	19.85
6	0.2187	21.78

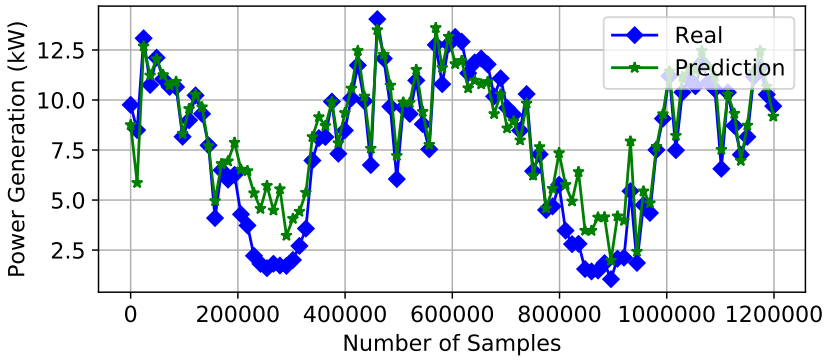

Figure 6.6: Real And Predicted Downsampled Generation.

introduced into the predictions increase largely. The difference of the prediction and real power generation with respect to months is also analyzed in Fig. 6.7. The analysis is expressed in the form of a histogram over five months of year 2015 with error bars indicating the variance in the prediction, from August to December.

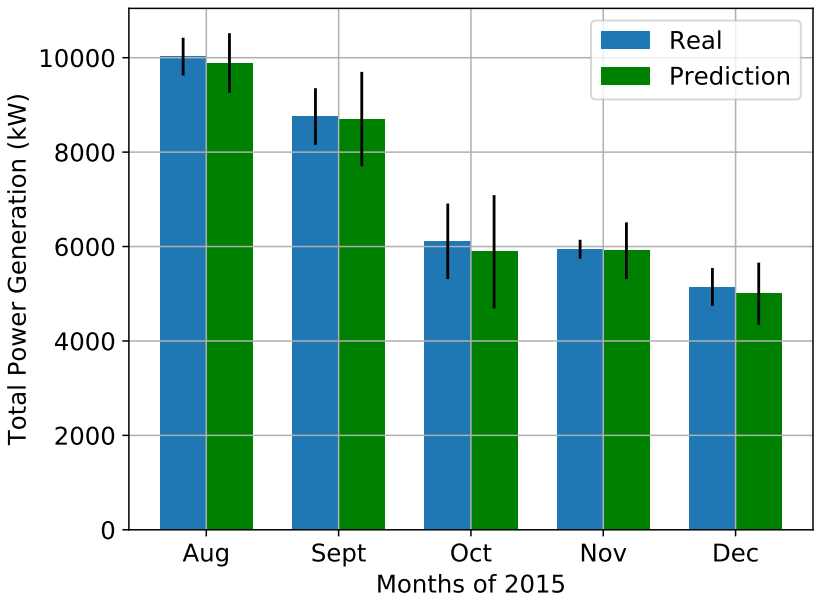

Figure 6.7: Histogram Of Accumulated Generations.

Chapter 7

PV ORIENTATION EFFECTS

7.1 Effects of PV Orientation Angles

There are some more observations, it is difficult to say that they would be universally true. But, prima facie, it can be said that when the solar panels are oriented towards true South then the total power generation over a whole year is generally the highest. The system that peaks closest to noon are taking most advantage out of the energy coming from the sun, in case of the systems that do not have any solar tracking. The southern most peaked closes to the mid value of the time which has to be close to 150 in the Figure 22. A potential explanation can be its orientation in the True South direction. Rest of them do not seem to be fully in True South direction and inclined. So, the farther the panels are from the True South, probably the farther their peak is from the noon point which in most cases is around 12:00 pm. The curves in Figure 22 are normalized from 0 to 1, in order to make their generations comparable. The points when they peak will be preserved in the process. Also, their naming is consistent with that of 7.2. For example, the blue curve in 8.1 show the normalized generation of the solar panels installed at the point labelled as North in 7.2.

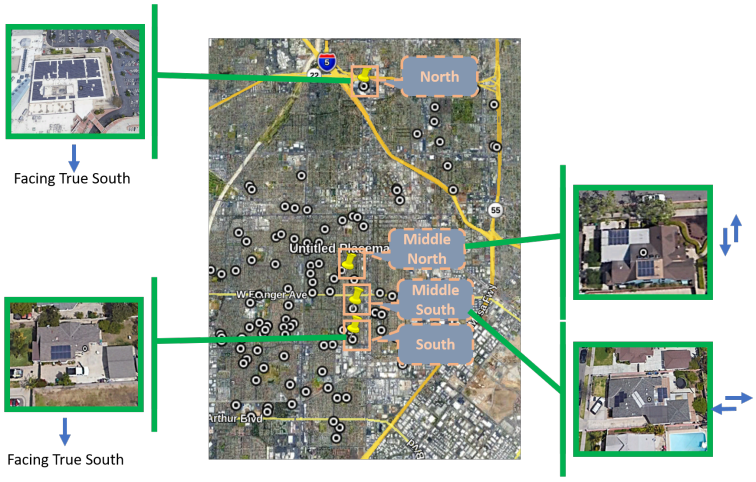

Figure 7.1: Orientation Angle Differences.

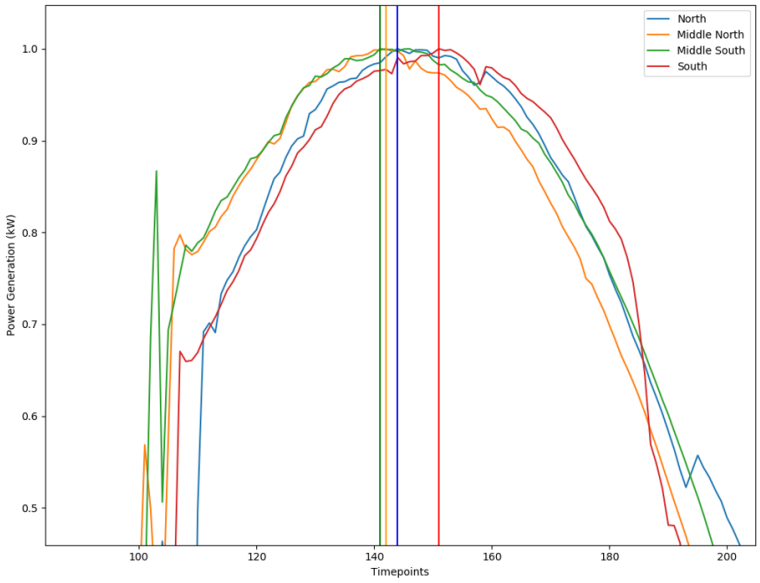

Figure 7.2: Voltage Variation.

Chapter 8

ARCING FAULT PROTECTION

At the early stage, enhancements of conventional relays are proposed, leading to a proportional relaying algorithm, impedance-based method, and PC-based fault locating and diagnosis algorithm. However, these methods are ineffective in detecting AFs with a low fault current. For this problem, harmonics patterns are utilized to capture AF characteristics, such as magnitudes and angles of 3^{rd} and 5^{th} harmonics, even order harmonic power, and interharnomic currents. Besides, a Kalman-filter-based method is proposed to monitor harmonics in AFDs. This type of method actively injects higher than fundamental frequency signals like positive/zero voltage signals into the grid for AFD. The solar power systems integrated into the grid makes the protection vulnerable to maloperation. The arcing fault protection in the distribution grid creates false tripping. Hence, a study is performed by incorporating the solar generation into the distribution grid. The protection scheme for arcing faults is developed and is presented in the North American Power Symposium.

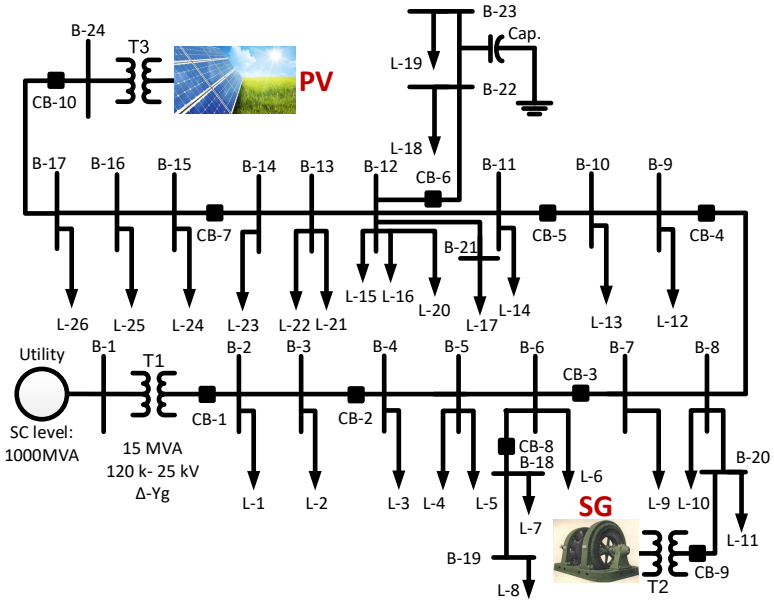

Figure 8.1: PV Integrated In Distribution Grid.

Chapter 9

LOW FREQUENCY DAMPING CONTROL

Inter-area oscillation problem is one of the major stability issues that face interconnection of the power systems. Recent development in wide-area measurement systems (WAMS) provides a great potential to overcome the shortcomings of conventional local controllers and it makes using of remote signals as inputs for controllers feasible. Literature provides a survey of recent research and developments in the field of wide- area control for inter-area oscillation damping. Moreover, new researchers can follow recent and future trends in the area of wide-area damping control system. The typical range of frequency lies between 0.1 -2.0 Hz.

WAMS has a significant advantage where a suitable architecture is selected. Such an architecture can help increase in stability and reliability of the power grid. The factors like PMU data acquisition, decision making based on PMU data and the enactment of actions based on decision making determine the architecture details of WAMS. Different combinations of such factors can direct towards different realizable types of WAMS architectures. This thesis focusses on the utilization of the WAMS architecture and the measurements to implement smart grid.

The damping of frequency oscillations requires a precise continuous control. Numerous kinds of Power System Stabilizers (PSS) have been widely used for the

control of frequency oscillations, but they are localized. Each generating unit have an independent PSS that takes in the localized inputs. The thesis proposes a wide area based damping control scheme. The WAMS based damping controller will take in the wide area inputs and generate control signals for different generating units simultaneously. The centralized control can provide a higher degree of flexibility. Moreover, a situational awareness of a wide area can help to come up with a better control strategy.

Chapter 10

MODELLING

Frequency oscillation control should have a continuous control signal. A specialized reinforcement learning (RL) based methodology is introduced in the thesis. There are several different types of machine learning algorithms, among them, are the reinforcement learning algorithms. RL algorithms are gaining popularity in the field of control systems. A major advantage of utilizing RL methods is that, the control element can learn from its environment. Transmission systems are highly reliable because of their mesh network. Such a network, pose modelling challenges, when a centralized control is to be designed. That leaves us with a reinforcement learning solution.

10.1 Deep Deterministic Policy Gradient

Deep Deterministic Policy Gradient (DDPG) has not only a continuous control but also is an off policy algorithm. The fundamental benefit provided by DDPG that is not in the other reinforcement learning algorithms is that it can have the continuous action spaces. DDPG is also called deep Q learning for continuous action spaces. It is a technique that learns both Q values and action values, concurrently. This technique has its basis in the conventional Q-learning as well as

deep learning. For the Q-learning part, Bellman's equation has been used to measure the value function $Q(s, a)$, where s is the state and a is the performed action. We can directly take the gradient of the policy set. As the name of the technique suggests that, it is a policy gradient method and policy π is itself the optimal set of applied actions to achieve the objective in minimum number of steps. There are two segments of such a technique. First one is the Q-learning side. If s' is the next state and a' is the next action, the the optimal action value function $Q^*(s, a)$ is given by a Bellman's Equation

$$Q^*(s, a) = \underset{s' \sim P}{E}[r(s, a) + \gamma \max_{a'} Q^*(s', a')], \tag{10.1}$$

γ remains the discounting factor and $s' \sim P$ shows the following state, $s^{'}$, is sampled by the environment from a distribution $P(\cdot|s, a)$. The value function approximator is $Q^*(s, a)$ is a comprises deep neural networks, that in the current scenario is a 3 neural network have 128 perceptrons in the first layer 32 in the second and 1 in the last layer.

We consider a standard reinforcement learning setup consisting of an agent interacting with an environment E in discrete timesteps. At each timestep t the agent receives an observation x_t, takes an action, receives a scalar reward r_t. Real valued actions are $a_t \in \mathbb{R}^N$. In general, the environment not be completely observed and the entire history of the observation, action pairs $s_t = (x_1, a_1, \cdots, a_{t1}, x_t)$ are necessary to have to show the states. The assumption of fully observed environment is used here, so $s_t = x_t$. The output or behavior of an agent is defined by a policy, ,

which is nothing but a mapping between the states and a probability distribution for all the actions $\pi : S \rightarrow P(A)$. We define environment as E which may also be stochastic at times. The problem is developed as a Markov Decision Process where state is S, action space is $A \in \mathbb{R}^N$, an initial state distribution $p(s_1)$, we also define the transition dynamics $p(s_{t+1|s_t}, a_t)$, finally there is a reward function $r(s_t, a_t)$. Using the state we can come up with a discounted future reward R_t having a discount factor $\gamma \in [0, 1]$. There is an important thing that the return relies on the chosen actions. The main objective in of reinforcement learning is to maximize the return reward,

$$J = E_{r_{i,s_i} \sim E, a_i \sim \pi}[R1]. \tag{10.2}$$

Here we have discounted state visitation distribution for a policy π as ρ^π. The action value function is used here, that describes that upon taking action what will be the expectation and new state s_t and thereafter following policy π,

$$Q = (s_t, a_t) = E_{r_i t, s_i > t \sim E, a_i > t \sim \pi}[R_t | s_t, a_t]. \tag{10.3}$$

Bellman equation is used in the iterative process to have the approximation for value function

$$Q = (s_t, a_t) = E_{r_t, s_{t+1} \sim E}[r(s_t, a_t) + \gamma E_{a_{t+1} \pi}[Q(s_{t+1}, a_{t+1})]. \tag{10.4}$$

If the target policy is deterministic we can describe it as a function $\mu : S \rightarrow A$,

$$Q(s_t, a_t) = E_{r_t, s_{t+1} \sim E}[r(s_t, a_t) + \gamma Q(s_{t+1}, \mu(s_{t+1}))]. \tag{10.5}$$

The expectation relies highly on the environment we are working in. Hence, we can learn Q^{μ} through simply getting an off-policy method, using transitions of policy β. Greedy policy is used in the Q-Learning algorithms. We assume function approximators parameterized by θ^{Q}, can have a solution by optimization techniques, where loss has to be minimized,

$$L(\theta^{Q}) = E_{s_t \sim \rho^{\beta}, a_t \sim \beta, r_t \sim E}[Q(s_t, a_t|\theta^{Q})] - y_t]^2, \tag{10.6}$$

where,

$$y_t = r(s_t, a_t) + \gamma Q(s_{t+1}, \mu_{(s_{t+1}}|\theta^{Q}), \tag{10.7}$$

while y_t is also dependent given θ^{Q}. The use of large, non-linear function approximators for learning value or action-value functions has often been avoided in the past since theoretical performance guarantees are impossible, and practically learning tends to be unstable. Recently, adapted the Q-learning algorithm in order to make effective use of large neural networks as function approximators. We employ these in the context of DDPG and explain their implementation in the domain of low frequency oscillation damping using the measurements from wide area measurement systems.

The architecture have the environment and reward blocks. The environment block has been developed on MATLAB Simulink.

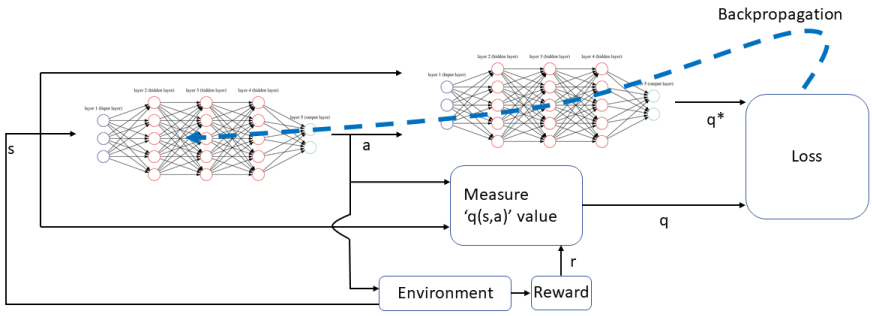

Figure 10.1: Architecture Of Deep Deterministic Policy Gradient Method.

Chapter 11

POWER SYSTEM MODELLING

The test system consists of two fully symmetrical areas linked together by two $230kV$ lines of $220km$ length. It was specifically designed in to study low frequency electro-mechanical oscillations in large interconnected power systems. Despite its small size, it mimics very closely the behavior of typical systems in actual operation. Each area is equipped with two identical round rotor generators rated $20kV/900MVA$. The synchronous machines have identical parameters, except for inertias which are $H = 6.5s$ in area 1 and $H = 6.175s$ in area 2. Thermal plants having identical speed regulators are further assumed at all locations, in addition to fast static exciters with a 200 gain. The load is represented as constant impedances and split between the areas in such a way that area 1 is exporting $413MW$ to area 2. Since the surge impedance loading of a single line is about 140 MW, the system is somewhat stressed, even in steady-state. The reference load-flow with M2 considered the slack machine is such that all generators are producing about $700MW$ each. The results can be seen by opening the Powergui and selecting Machine Initialization. They are slightly different from benchmark two area system, because the load voltage profile was improved (made closer to unity) by installing $187Mvar$ more capacitors in each area. In addition, transmission and generation losses may

vary depending on the detail level in line and generator representation.

11.1 Simulation

For an initial understanding of the network behavior, we can simulate its open-loop responses (PSSmodel = 0) to a 5%-magnitude pulse, applied for 12 cycles at the voltage reference of M1. This test is activated by opening the timer controlling the voltage reference of M1 and changing the multiplication factor of the transition times vector from 100 to 1. Similarly, the line fault should be deactivated by changing from 1 to 100 the multiplication factor of the transition times vector in the ”Fault” device and line breakers ”Brk1” and ”Brk2”. After starting the simulation, the signals responses are visualized by opening the ”Machine” and ”System” scopes on the main diagram. All signals show undamped oscillations leading to unstability. A modal analysis of acceleration powers of the four machines shows three dominant modes,

1. An interarea-mode ($fn = 0.64Hz, z = -0.026$) involving the whole area 1 against area 2: this mode is clearly observable in the tie-line power displayed in ”System” scope

2. Local mode of area 1 ($fn = 1.12Hz, z = 0.08$) involving this area’s machines against each other

3. Local mode of area 2 ($fn = 1.16Hz, z = 0.08$) involving machine M3 against M4 (i.e.: the smaller the inertia, the greater the local natural frequency)

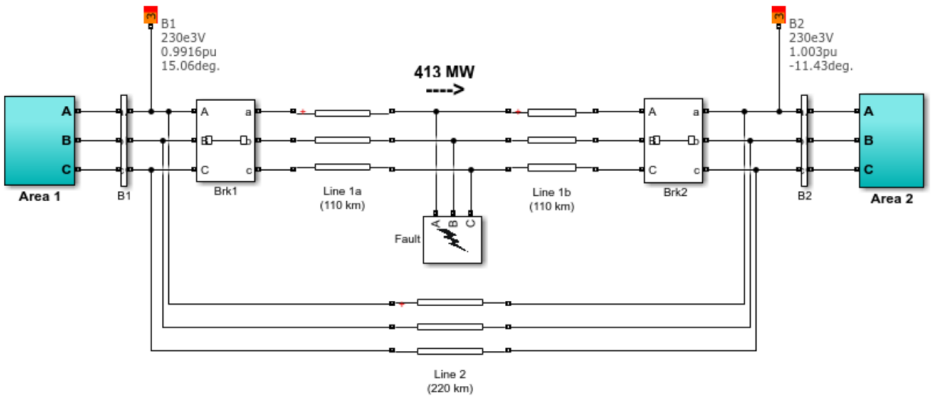

Figure 11.1: Wide Area Model Principles.

If one of the two tie-lines is removed by setting the breakers ”Brk1” and ”Brk2” in an open position, it is possible to achieve another steady-state stable equilibrium point with the same generation and load patterns. This is called a post-contingency network, easy to initialize using the Machine Initialization tool of the Powergui. A modal analysis of this network's responses to the same 5%-magnitude pulse, applied for 12 cycles at the voltage reference of M1 reveals that, while the two local modes remain basically unchanged in both frequency and damping ($fn = 1.10Hz, z = 0.09$ in area 1 and $fn = 1.15Hz$, $z = 0.08$ in area 2), the interarea mode shifts to a much lower frequency with still a negative damping (i.e.: unstable): ($fn = 0.44Hz, z = -0.015$).

The result of DDPG based wide area control of the four generator system show that there is a better control of the system, whereas the conventional PID (Proportional Integral and Derivative) controller can not handle the time delays if they keep varying. The DDPG based controller can learn on the distribution of the time

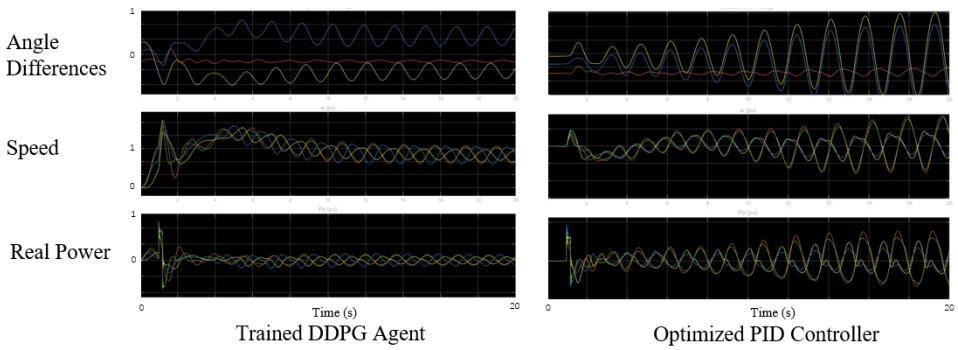

Figure 11.2: DDPG-Based Control And PID control.

delays also. As the Fig. 11.2 indicates the the speed of the generators in the trained DDPG model remain consistent for longer period of time, in contrast to what we see in the PID controller based control, where the speed goes on increasing and the oscillations in the system will ultimately enforce the system to lose synchronism.

Chapter 12

EFFECTS OF TRANSIENT OVERVOLTAGE (TOV)

The three pilot protection schemes applied for cable protection are current differential, phase comparison, and directional comparison. Backup protection of underground cables is provided using phase distance, directional ground over-current, or ground distance protection.

The most common protection for circuits consisting of underground cables only is line current differential. Typically, in such a circuit, two-line current differential relay schemes, a Main One and a Main Two system, are applied, each one interfacing with a digital communications channel connected to separate and independent communications paths. This application could also have direct transfer tripping for breaker failure conditions on the same digital channels, taking advantage of relay-to-relay communications. Autoreclosing is not typically allowed because the protective circuit consists of an underground cable only.

Quite often, EHV cable circuits terminate in transformers to serve the load of a major metropolitan area. In such applications, the Main One and Main Two cable protection systems could consist of either current differential protection and/or directional comparison protection schemes, using phase distance and negative-sequence directional elements for sensitive ground fault protection. In these types

of applications, we can take advantage of digital relay-to-relay communications and send the direct transfer trip (DTT) bits for transformer faults to the remote station using the same digital channels that are used for the line current differential or the directional comparison scheme.

One important difference from cable circuits is that many users allow high-speed reclosing if the overhead line length is much greater than the underground cable length. Systems where the cable length is less than 15 to 25 percent of the total circuit length may have autoreclosing. Another important factor is whether the cable portion is at the beginning of either terminal or whether it is between two overhead line sections.

If the cable is at the beginning of the transmission line, and the line length is much longer than the cable section length. In Fig. a, at the terminal farther away from the cable, the distance relay has only one Zone 1 element (Z1). The reach of this element is set at 80 percent of the overhead line positive sequence impedance. Operation of this element trips the local breaker, sends a DTT to trip the remote breaker, and allows high-speed reclosing. Operation of the overreaching Zone 2 element (Z2) trips the local breaker and blocks its high-speed reclosing.

If the underground cable is of the pipe type, reclosing may be prohibited unless line current differential schemes are protecting the cable portion separately, as shown in Fig. b. In such a case, we can positively identify that the fault is on the cable circuit and, via communications, block autoreclosing at the two ends of the

line.

When the cable is very short (for instance, less than 300 meters) and not a pipe-type cable, some users ignore the cable and allow high-speed reclosing because they assume that the majority of the faults will be on the overhead line section. In some cases, it is economical for short cable lengths to be thermally dimensioned for autoreclosing. However, for longer cable lengths, autoreclosing may or may not be feasible, depending on the thermal rating of the cable. A three-terminal application in which the cable is protected by a separate line current differential scheme for high-speed detection of cable faults and for blocking highspeed reclosing at the other two terminals.

The underground transmission cables differ drastically from their overhead counterparts. These cables have sheaths and shields that are grounded along cable length. Due to magnetic coupling of phase currents and among currents in cable sheaths complex calculations are involved in computation of series impedances. Ground fault can have multiple return paths like the sheath, the ground or a combination of both [1].

- One limitation of symmetrical component theory is the assumption that power system element impedances are balanced. This is not true in underground cables because of the different methods used for cable sheath bonding and grounding [1].

- Another difficulty in applying symmetrical component theory is the require-

ment to retain the sheaths, including their transpositions and grounding along the cable path, to properly study faults along the entire cable length or mixed conductor technology circuit [1].

- The positive-sequence impedance of underground cables is much lower than the positive-sequence impedance of overhead lines in ohms per unit of length. In some cases, the total cable circuit positive-sequence impedance may be less than the minimum distance relay setting range value.

- The cable zero-sequence impedance angle is also much lower than the zero-sequence impedance angle for overhead lines.

- The presence of water pipes, gas pipes, railways, and other parallel cables makes the zero-sequence current return path rather complex.

- The zero-sequence impedance may be nonlinear with respect to distance.

Capacitance causes current to flow even when no load is connected to the cable. This is called line charging current. Underground line capacitance for power cables is far higher as compared to their overhead counterparts due to closeness of cables and proximity to earth. As a result, underground lines have 20-75 times the line charging current.

Switching transient in power systems is related to the operation of breakers and switches. Among others, the switching surges usually occur upon the energization of lines, cables, transformers, reactors, or capacitor banks. An underground cable

Figure 12.1: Cable Failure For Underground System.

Figure 12.2: Cable Failure In Salt River Project.

must be protected against excessive overheating caused by fault currents. Excessive heating could damage the cable, requiring lengthy and costly repairs. Because most cable faults involve ground initially, ground fault protection sensitivity is of utmost importance. Long underground cable circuits produce high charging cur-

rent, which may be an appreciable fraction of the load current. Cable circuit energization and de-energization create high transient currents. Similar high transient discharging and charging currents flow in the cable circuit during faults external to the cable zone of protection.

Upon de-energization, which is usually associated with the fault clearing devices, switching transients prevail as well. Therefore, it is interesting to investigate the effects of reclosing, especially the resulting overvoltage phenomenon in an electric network, for the practical consideration of eliminating the occurrence of cable failure.

Chapter 13

TEMPORARY OVERVOLTAGE PHENOMENON

One of the reasons for the failure of cable is transient over-voltages. Transient over-voltage can arise from the supply or from switching inductive loads, harmonic currents, d.c. feedback, mutual inductance, high-frequency oscillations, large starting currents and large fluctuating loads. Transient over-voltages (TOV) or surges are temporary high magnitude voltage peaks for a short duration of time, ex: Lightning. Switching transients in electrical networks often occur. Although the voltage magnitude is lower than lightning surge, the frequency at which it occurs causes ageing of cable insulation and eventually breaks down resulting in flashover.
Besides the aforementioned concerns, the investigation of the effects of reclosing cannot be conducted without taking into consideration of the following mechanisms that cause TOVs:

- Ground potential rise;
- Derived neutral shift;
- Inductive coupling of fault currents;
- High generation to load ratio;
- Interruption of inductive currents;

- Over-modulation/saturation of current.

The main TOV source in our network is from mechanism 2 the derived neutral shift, which usually involves single-phase-to-ground fault. When the associated substation breaker opens upon the fault, the phase conductors might be floating due to the absence of the ground potential reference. Therefore, during a fault, the unfaulted phases would have a phase-to-ground voltage magnitude equivalent to phase-to-phase voltage (1.73 times their rated voltages). Moreover, distributed energy resources (DERs), especially inverter-interfaced DERs, are weak in maintaining three-phase balanced voltages. Unlike synchronous machines, what the inverter-interfaced DERs can maintain is the balanced three-phase currents. Therefore, the main TOV source in distribution network originates from upstream substation.

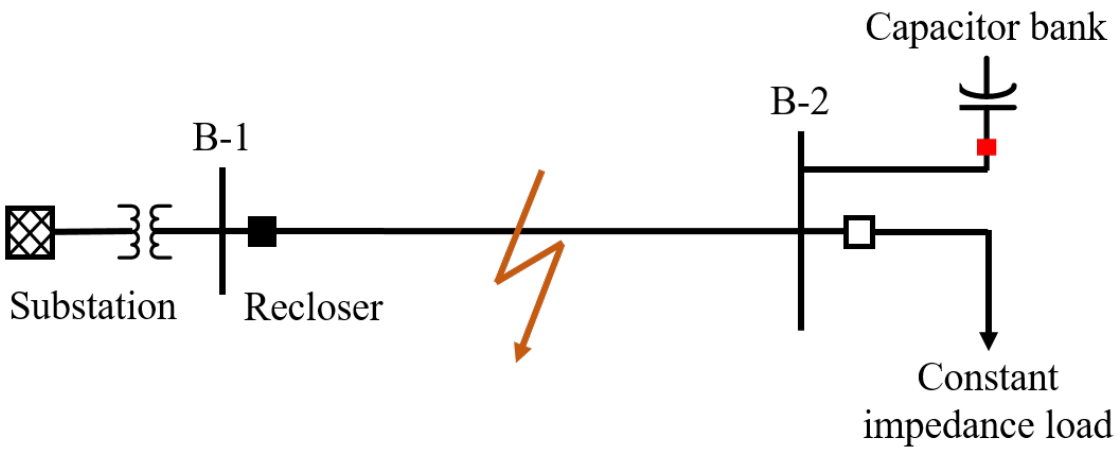

Figure 13.1: Benchmark System Under Study.

Such an over-volatge will keep on causing stress in the distribution cables and

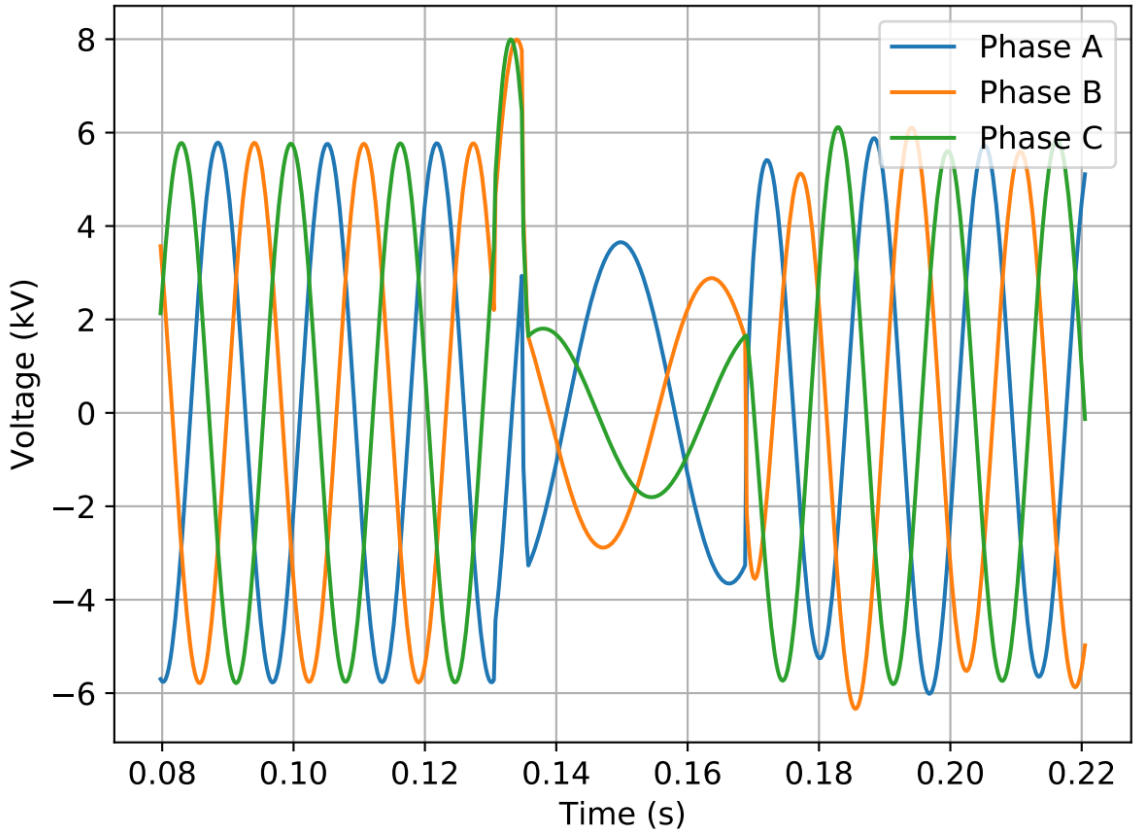

Figure 13.2: Developed TOV at 0°.

can ultimately lead to the insulation rupture or line failure.

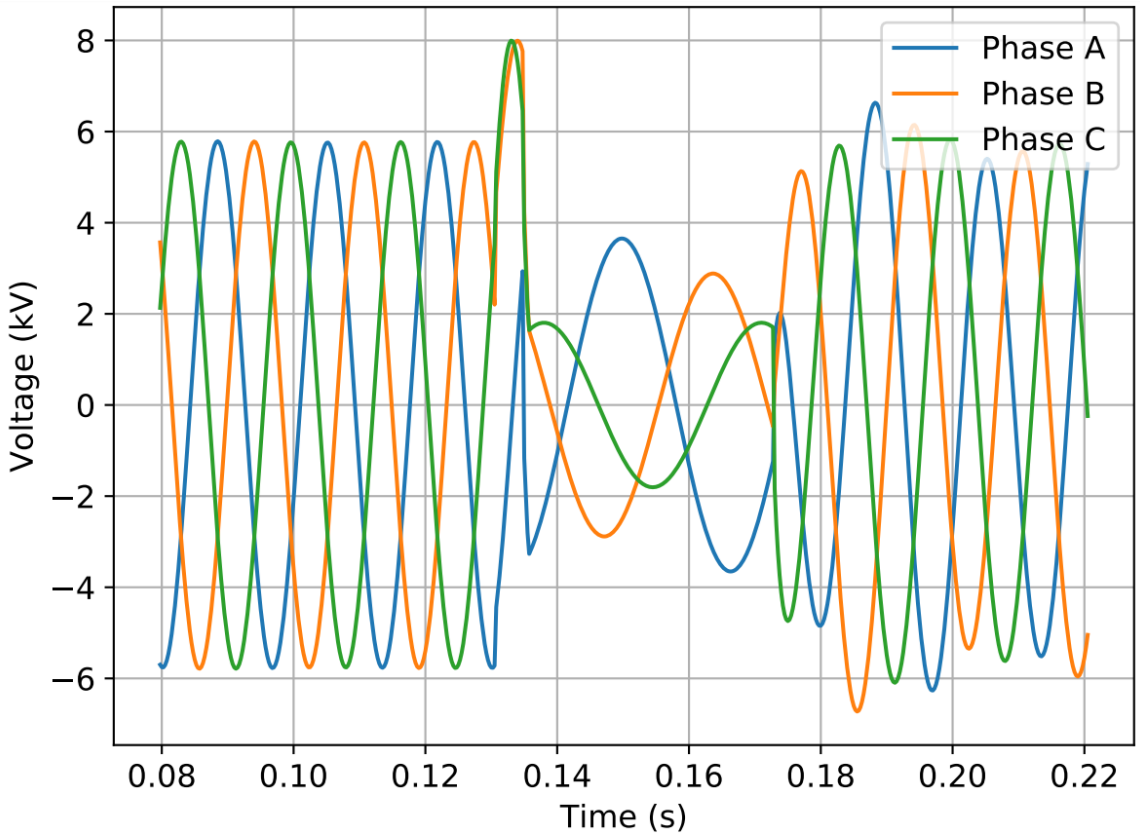

Figure 13.3: Developed TOV at 90°.

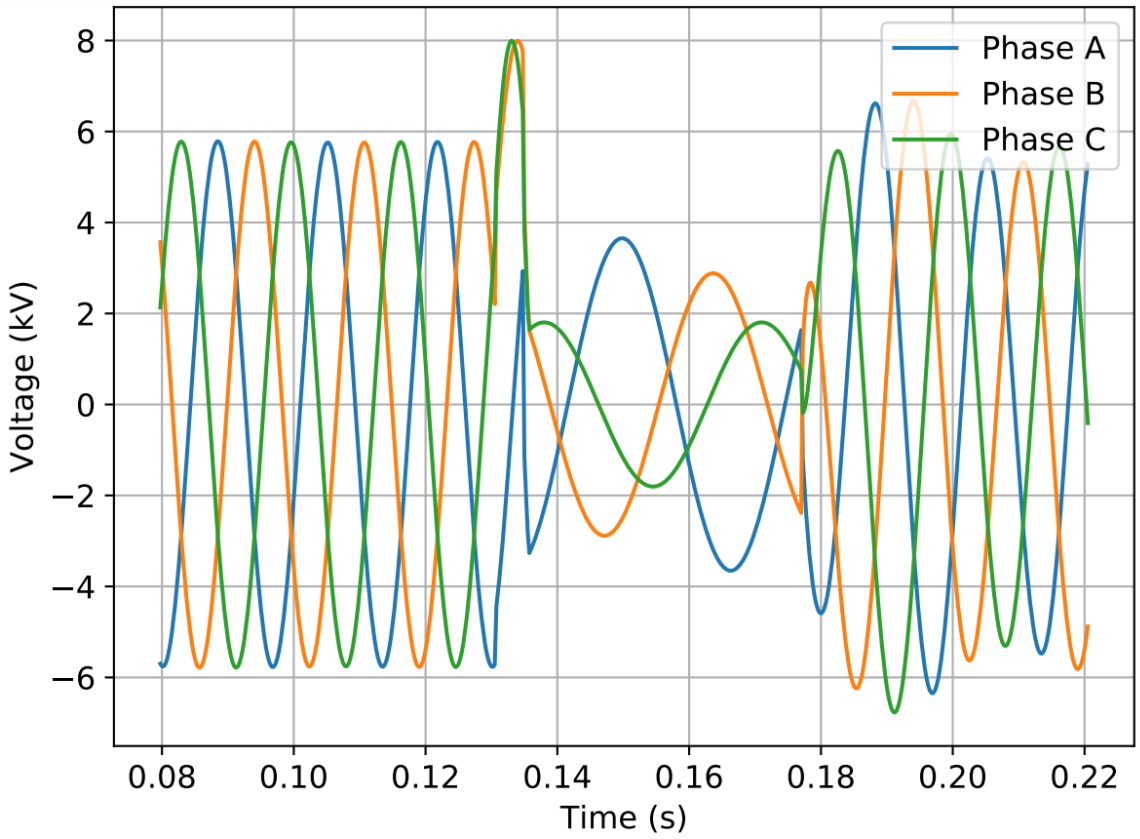

Figure 13.4: Developed TOV at 180°.

Chapter 14

REINFORCEMENT LEARNING ENVIRONMENT

For each phase $p \in \{0, 1, 2\}$ there are voltage and current measurements from the bus, located downstream of the breaker under study. The magnitudes of voltage $|V_p|$ and current $|I_p|$ along with the voltage phase angle θ_{V_p} and current phase angle θ_{I_p} of the measurements are considered for defining a 4-dimensional state space s of the system

$$s = \begin{bmatrix} |V_p| \\ \theta_{V_p} \\ |I_p| \\ \theta_{I_p} \end{bmatrix}. \tag{14.1}$$

Additionally, we define action space of the controlling system, that suits the system and can deliver best results. Therefore, we select a binary action space $a \in \{0, 1\}$. Here, 0 indicates that the recloser is open, whereas 1 indicates that it is closed.

The reward comprises two parts, the TOV-related reward and the temporal sequence reward. The TOV can by getting the deviaiton from the reference voltage of 1 pu. Whereas, the task sequencing can be achieved by having the enablin ghte model to learn on the number of distinct action sequences, to achieve the desired policy.

We define the reward function as R_i using an indicator function that can en-

able the function to generate a high value only when the desired task sequence is achieved. Here $Ind(I_d^{(t)} > 0, I_p^{(t)} < 0)$ is an indicator function which is 1 when $I_d^{(t)} > 0$ and $I_p^{(t)} < 0$ are true and is 0 otherwise. That helps the model in learning not to reclose before the first opening operation takes place. Whereas, once the reclosure takes place in a desired time range, the rms value of three phase voltage helps in keeping the transient overvoltage in check, by making sure that the deviation from the reference is reduced.

$$R_i = \alpha \cdot \text{Ind}(I_d^{(t)} > 0, I_p^{(t)} < 0) - \text{Ind}(I_d^{(t)} > 0, I_p^{(t)} < 0) \cdot \beta \cdot (|V_d^{(t)} - V_{ref}|) \quad (14.2)$$

Where the indicator function is the representation of the capability of the task sequencing. For example, the operation for a particular breaker can be limited to a fixed number by updating the indicator function. For the first part the model should be capable of reclosing only once, while keeping the TOV limited.

Based on the problem formulation in Section aaaaa and the complexity of the electric grids, we find that the policy iteration method needs to involve intensive use of simulation for the parametric approximation. To enable self-learning of the protective relays, an actor-critic system [38] is adopted for approximate policy evaluation. The *critic* in this system evaluates the policy, and the *actor* is the algorithm that improves the policy value. We use μ^k to denote the kth policy, and $\tilde{J}_{\mu^k}$ to quantify the kth policy. The actor-critic method generates a sequence of stationary policies $\{\mu^k\}$ and a corresponding sequence of the approximate pol-

icy evaluation $\{\tilde{J}_{\mu^k}\}$ using simulation software such as Matlab, PSCAD, etc. The actor-critic method update its current policy μ^k to μ^{k+1} through the following minimization:

$$\mu^{k+1}(i) \in \arg\min_{u \in U(i)} \sum_{j=1}^{n} p_{ij}(u)(g(i,u,j) + \alpha \tilde{J}_{\mu^k}(j)) \tag{14.3}$$

Alternatively, the system can compute the minimizing control u^s at a set of sample states i^s, $s = 1, \cdot, q$, through

$$\mu^s \in \arg\min_{u \in U(i^s)} \sum_{j=1}^{n} p_{i^s j}(u)(g(i^s,u,j) + \alpha \tilde{J}_{\mu^k}(j)). \tag{14.4}$$

We propose to use system identification and simulation to construct a mathematical model of the system, including the current line topology, DER connectivity, operation mode (microgrid or grid-connected), and grounding types. Then we use the simulation-based policy iteration method update the protective relay settings. Since the probability of the system contingency events is rare, we introduce the importance sampling technique to overcome the large variance issue.

14.0.1 Deep reinforcement learning

Refer to Matlab examples: Preprocessing and Feature Extraction, Signal Generation and Acquisition https://www.mathworks.com/solutions/deep-learning/deep-learning-signal-processing.html

However, the system operator lacks of the information on the probability of

relay malfunctioning. Issues like cascading relay failure arise. Typically, the interaction loop between the agent and the environment is closed since the agent's action affects the state of the environment. Therefore the control loop is not closed. To address this problem, we ... The environment is affected by the agent's action that cannot be forecasted [39].

Deep Q-Learning with Experience Replay is shown in detail in [39].

Later, we can have the transfer learning part for the reward function. In order to achieve that we are trying to have the reward function also fitted in a polynomial line. Such a polynomial fitting helps to keep the reward function saved for the later use.

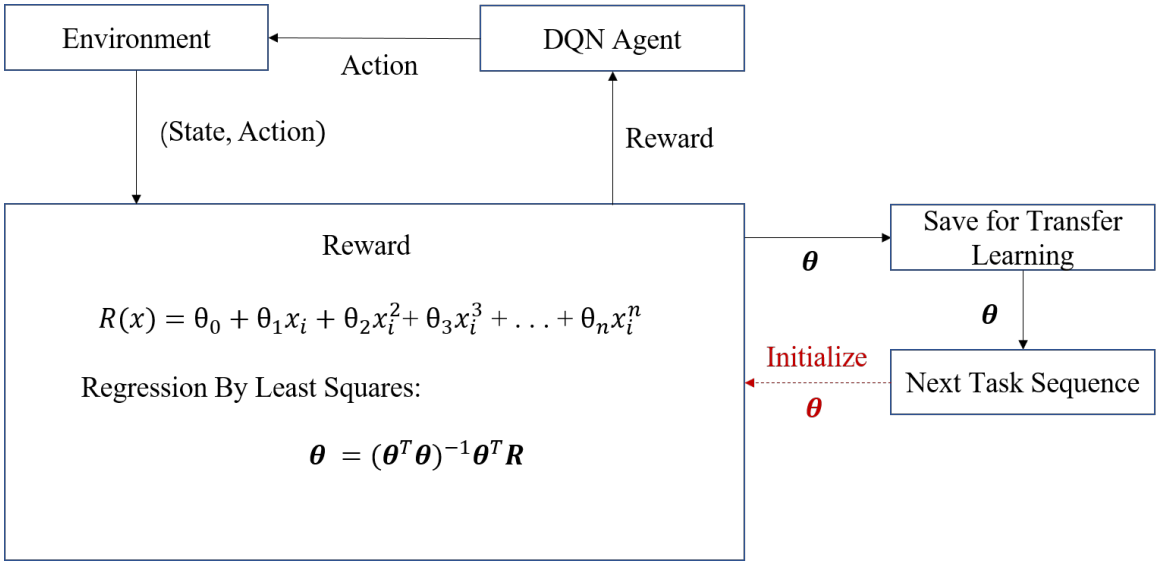

Figure 14.1: Transfer Learning.

Chapter 15

NUMERICAL VALIDATION OF BREKER CONTROL

The breaker control is performed through the DQN agent. The purpose int o tlearn the reclosure time so that the reward is maximized and the TOV is minimized.

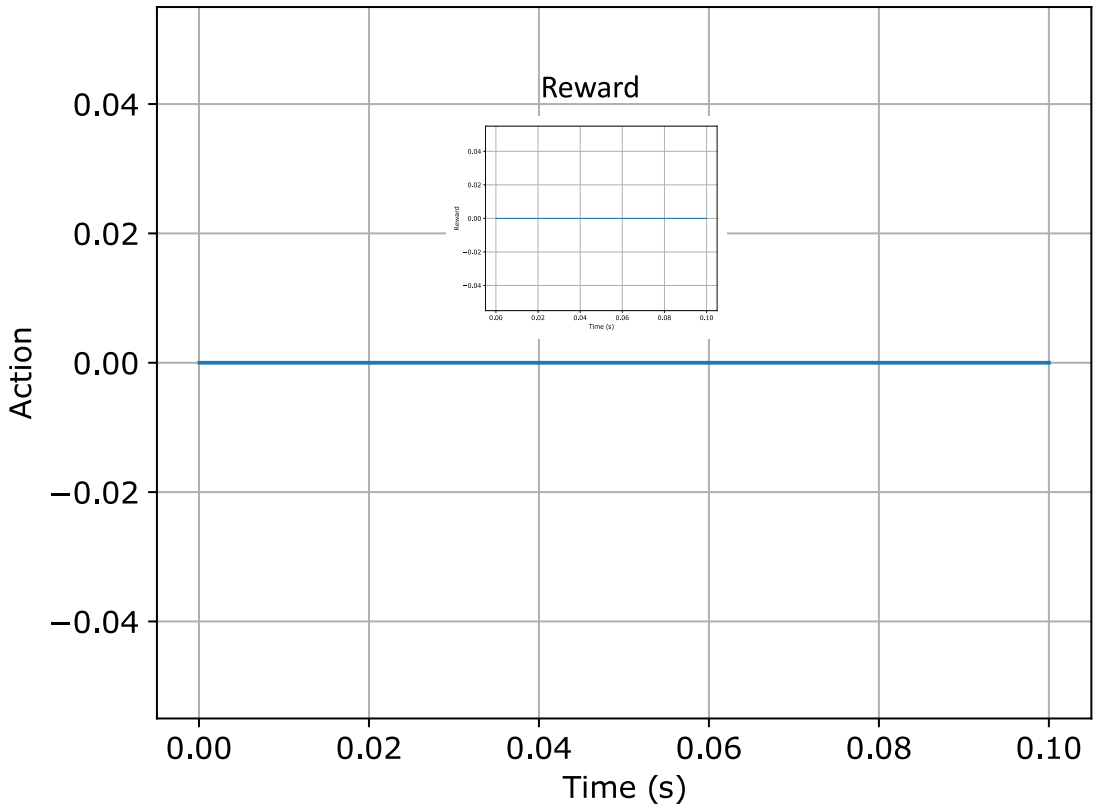

Figure 15.1: No Reclusure.

The above reclosure times show that actually the model is able to learn that the reclosure should take place at the optimal time. Since, the reclosure time is taking

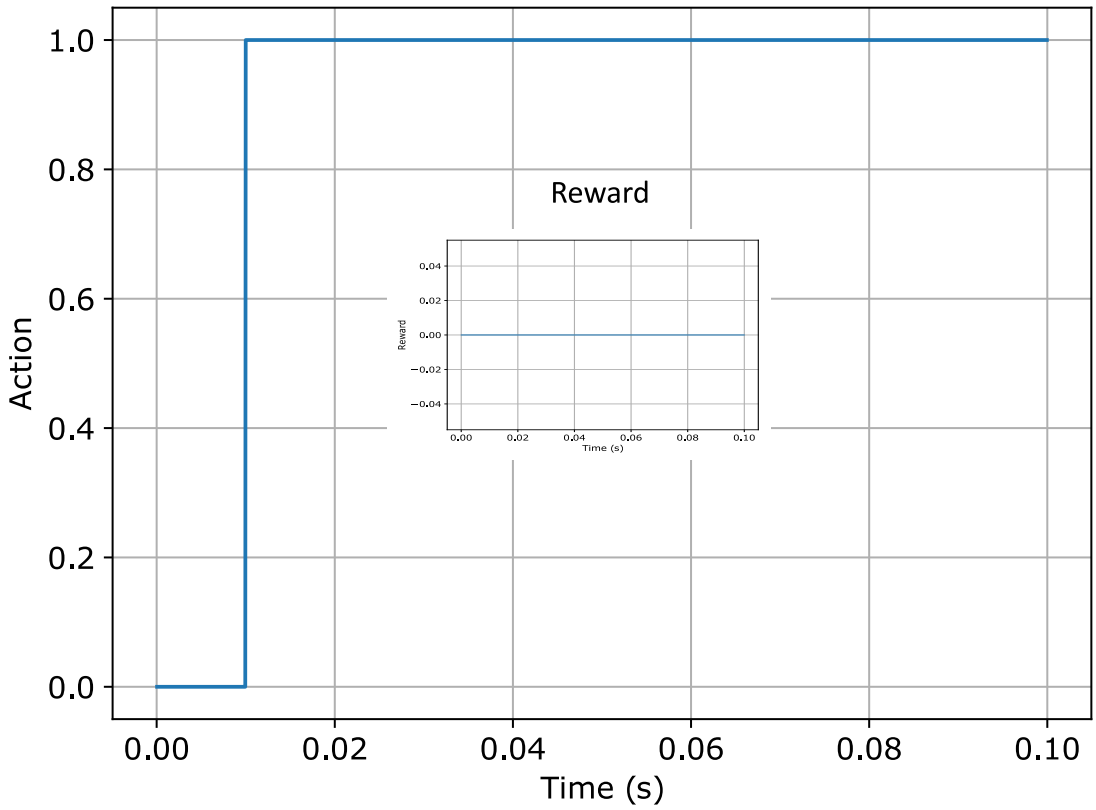

Figure 15.2: Reclosure Too Early.

place the time when the TOV is reduced in other words, the reward is maximized. Such an effect can be extended to more complex scenarios where the complexity of model can be increased further. Such as the task sequences are increased. There can be more tasks like multiple reclosures. Then, Such a learning can be done over a period of time by running th eenvironment for 1000 episodes and then using then constantly learning the parameters of the Deep Q Netowk model.

For showing the effect of hyperparameters we trained the model for $1,000$ episodes each and then check the variation of the Epsilon used in the epsilon

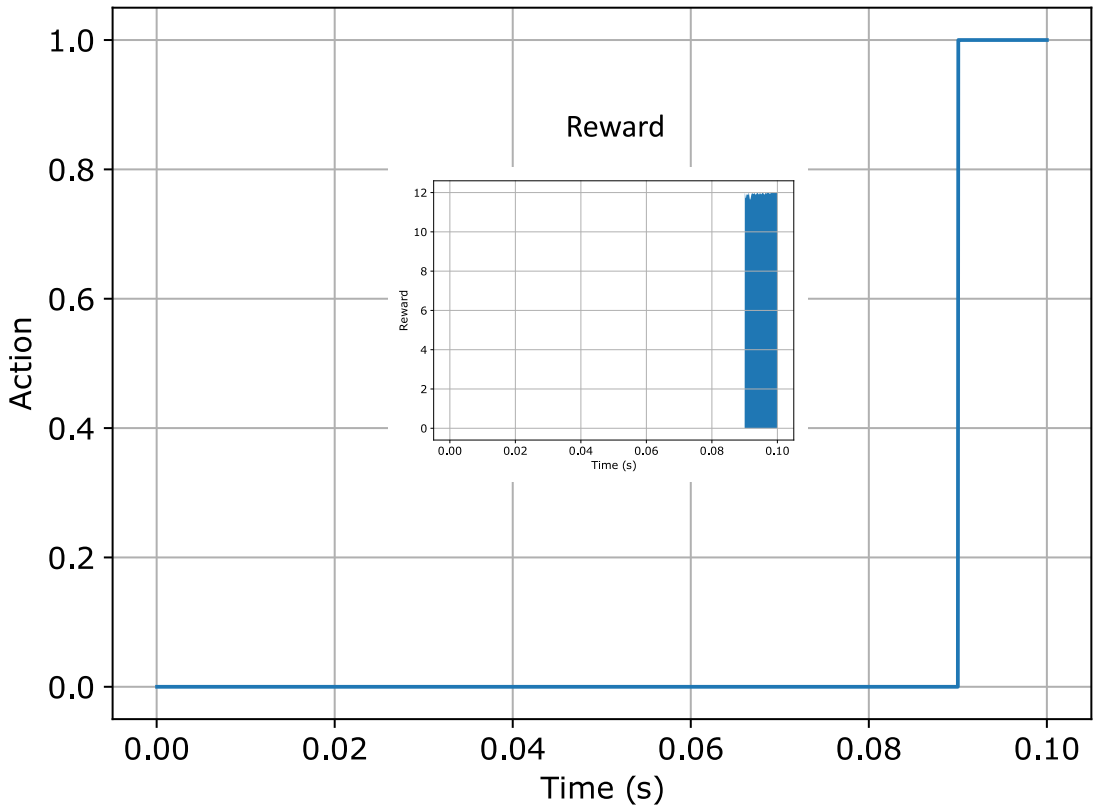

Figure 15.3: Reclosure Too Late.

greedy algorithm and also the discounting factor.

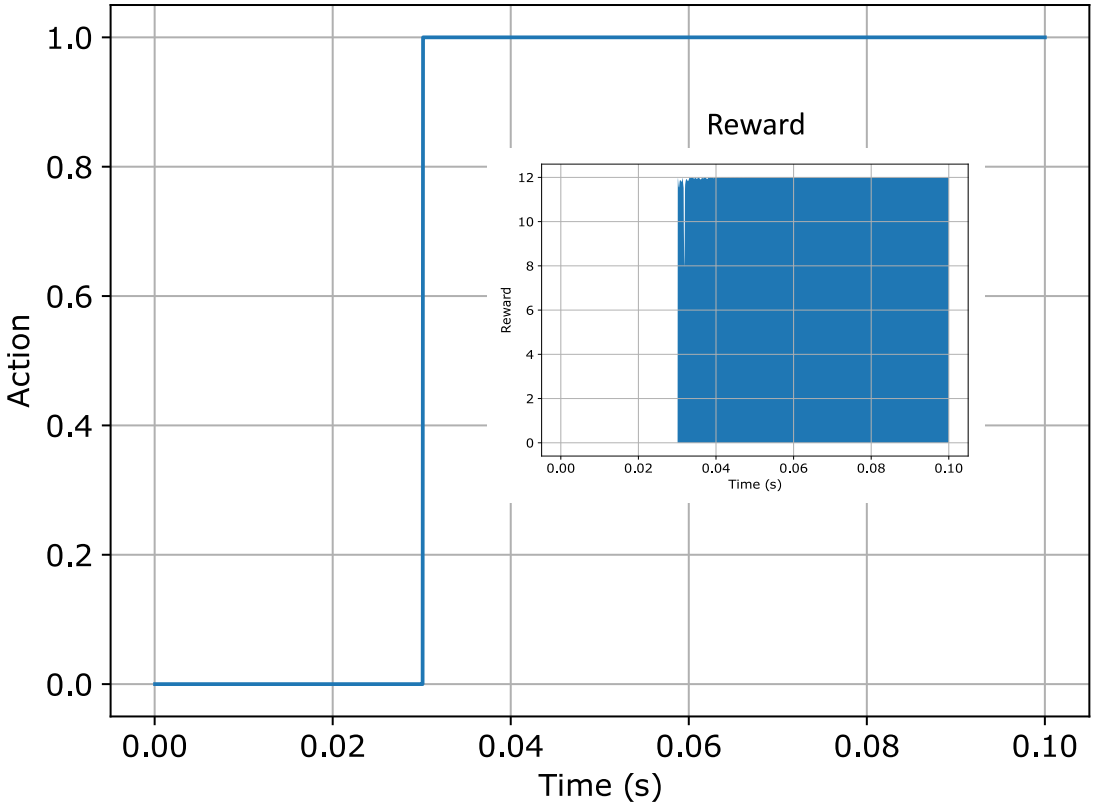

Figure 15.4: Reclosure At Optimal Time.

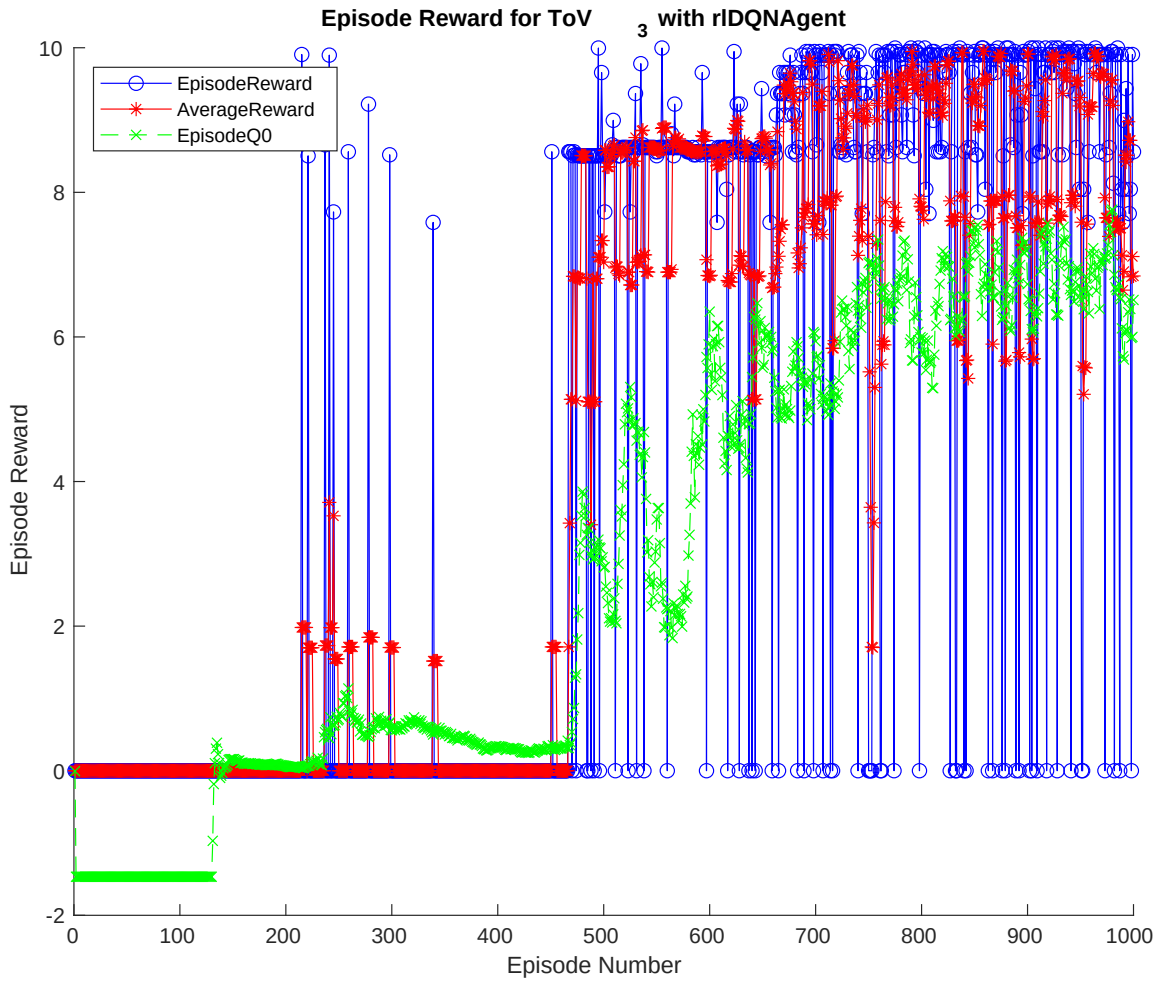

Figure 15.5: Learning Curve.

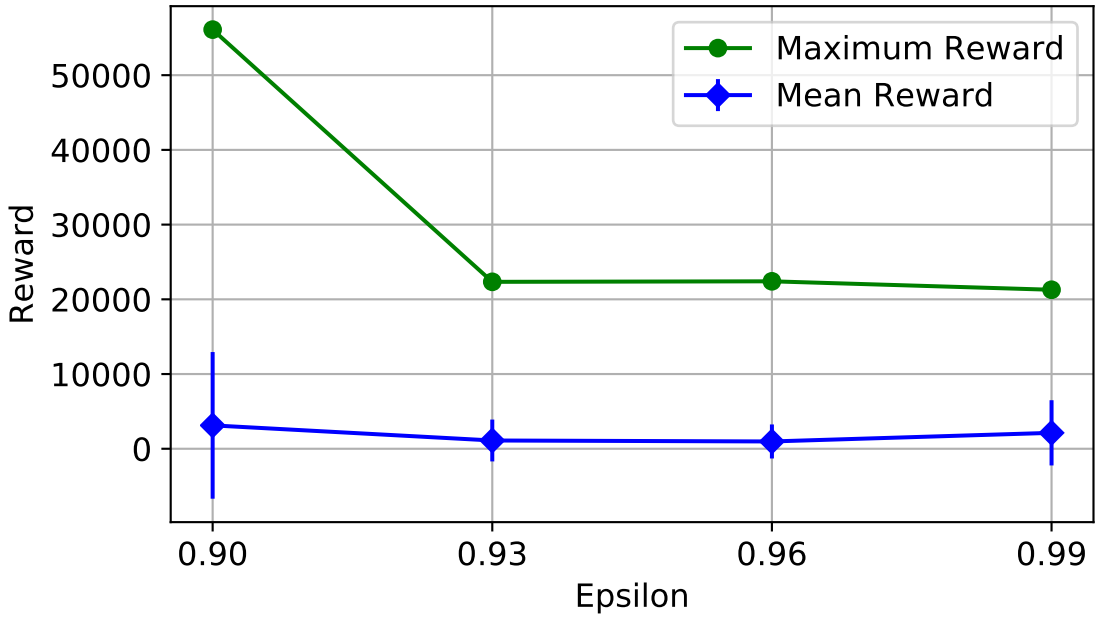

Figure 15.6: Effect Of Epsilon On Reward.

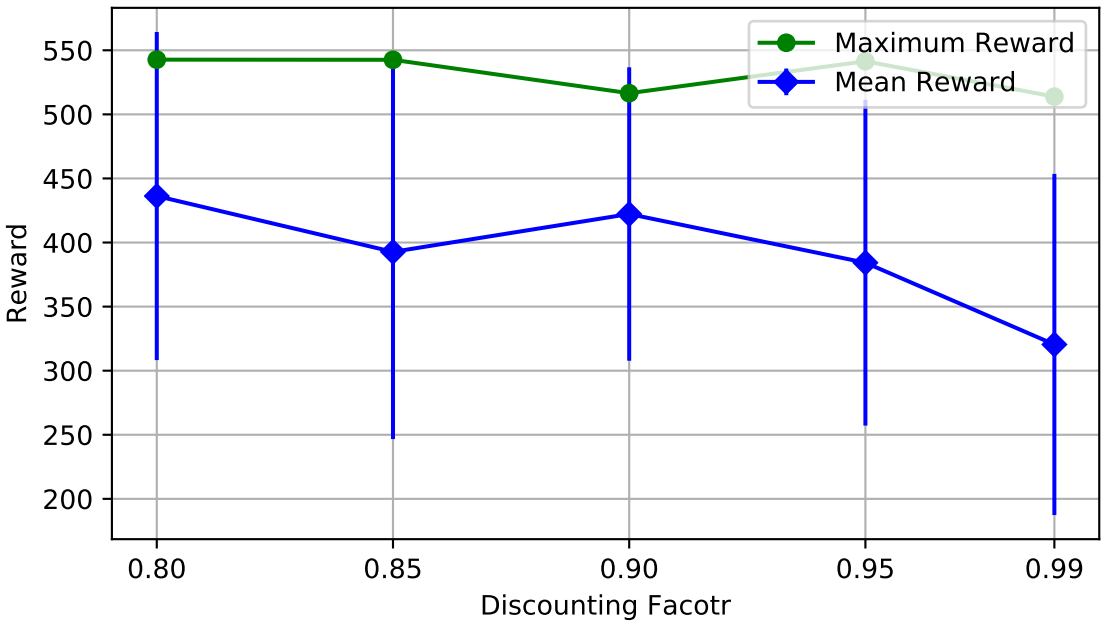

Figure 15.7: Effect Of Discounting Factor On Reward.

Chapter 16

CONCLUSION

In order to achieve better situational awareness to ensure smooth operation and control of distribution grids under high bidirectional power flows, we developed a mechanism by maximizing information gain through combining private data clouds with public sources. The method involves a detailed and carefully designed model to locate the solar modules and quantify them by overcoming the challenges of limited ground truth and low accuracy through rotation of the circular image slices and semi-supervised method for labelling randomized synthetic images. The quantity of modules and PV system generation data of neighboring solar power systems help to estimate the short-term as well as long-term generation of PV systems through selecting relevant features and employing KNN approach. High accuracy of results through comprehensive validation process helps to prove the concept, feasibility, and scalability of the proposed methodology. Thus, we achieve reliable operation and robust control of distribution systems. With better situational awareness and measurement capability, we need a better and more robust control at the distribution and transmission systems. For transmission systems the wide area damping control through reinforcement learning based DDPG Agent shows a promise especially to overcome the time delays in the communi-

cations. The distribution grid also needs to have a robust control strategy. Such a controlling strategy is built for the reclosers. The DQN based controller is designed for the reclosers so that the temporary over-voltage is mitigated.

REFERENCES

[1] D. A. Sunter, S. Castellanos, and D. M. Kammen, "Disparities in rooftop photovoltaics deployment in the united states by race and ethnicity," *Nature Sustainability*, vol. 2, no. 1, pp. 71–76, 2019.

[2] P. A. Basore and W. J. Cole, "Supply and demand constraints on future PV power in the USA," in *IEEE Photovoltaic Specialist Conference*, 2017, pp. 2163–2166.

[3] N. Srisaen and A. Sangswang, "Effects of PV grid-connected system location on a distribution system," in *IEEE Asia Pacific Conference on Circuits and Systems*, 2006, pp. 852–855.

[4] X. Buqiong and L. Yan, "Study on the impact of PV connection to grid on power flow based on time series output characteristics," in *IEEE Chinese Control Conference*, 2018, pp. 8991–8993.

[5] F. Foiadelli, S. Leva, and D. Zaninelli, "PQ and protection system analysis of a new topology for grid connected PV plant," in *IEEE International Conference on Clean Electrical Power*, 2011, pp. 243–248.

[6] Z. Chi, L. Pandian, Z. Xueying, Z. Jie, Z. Wei, H. Jiajian, X. Yu, and X. Qi, "Research on the impacts of grid-connected distributed photovoltaic on load characteristics of regional power system," in *International Conference on Green Energy and Applications*, 2017, pp. 95–99.

[7] V. Gupta, P. Raj, and A. Yadav, "Investigate the effect of dust deposition on the performance of solar PV module using LABVIEW based data logger," in *IEEE International Conference on Power, Control, Signals and Instrumentation Engineering*, 2017, pp. 742–747.

[8] P. Kadar, K. Attila, M. Andras, and S. Ervin, "Extension of the standard scada functionality with ai tools," in *PowerTech Budapest 99. Abstract Records.*, 1999, pp. 27–30.

[9] Z. Zhang, Q. Wang, Z. Chen, and A. Dubey, "Optimal strategies for scheduling the hourly demand response considering uncertainties of renewable energy in day-ahead market," in *IEEE International Conference on Probabilistic Methods Applied to Power Systems*, 2018, pp. 1–6.

[10] M. Alanazi, A. Alanazi, and A. Khodaei, "Long-term solar generation forecasting," in *IEEE PES Transmission and Distribution Conference and Exposition*, 2016, pp. 1–5.

[11] H. Zhou, Y. Zhang, L. Yang, and Q. Liu, "Short-term photovoltaic power forecasting based on Stacking-SVM," in *International Conference on Information Technology in Medicine and Education*, 2018, pp. 994–998.

[12] M. Yesilbudak, M. Çolak, and R. Bayindir, "A review of data mining and solar power prediction," in *IEEE International Conference on Renewable Energy Research and Applications*, 2016, pp. 1117–1121.

[13] Y. Liao, Y. Weng, G. Liu, and R. Rajagopal, "Urban MV and LV distribution grid topology estimation via Group Lasso," *IEEE Transactions on Power Systems*, vol. 34, no. 1, pp. 12–27, 2019.

[14] A. Fleischhacker, H. Auer, G. Lettner, and A. Botterud, "Sharing solar PV and energy storage in apartment buildings: resource allocation and pricing," *IEEE Transactions on Smart Grid*, vol. 10, no. 4, pp. 1–1, 2018.

[15] S. Lohar, R. Hirpara, T. Kalsara, and S. Patil, "Analysis and positioning of 2d solar panel," in *International Conference on Smart City and Emerging Technology*, 2018, pp. 1–5.

[16] J. M. Malof, Rui Hou, L. M. Collins, K. Bradbury, and R. Newell, "Automatic solar photovoltaic panel detection in satellite imagery," in *International Conference on Renewable Energy Research and Applications*, 2015, pp. 1428–1431.

[17] V. Golovko, A. Kroshchanka, S. Bezobrazov, A. Sachenko, M. Komar, and O. Novosad, "Development of solar panels detector," in *International Scientific-Practical Conference Problems of Infocommunications. Science and Technology*, 2018, pp. 761–764.

[18] H. S. Jang, K. Y. Bae, H. Park, and D. K. Sung, "Solar power prediction based on satellite images and Support Vector Machine," *IEEE Transactions on Sustainable Energy*, vol. 7, no. 3, pp. 1255–1263, 2016.

[19] M. Copur, B. M. Ozyildirim, and T. Ibrikci, "Image classification of aerial images using CNN-SVM," in *Innovations in Intelligent Systems and Applications Conference*, 2018, pp. 1–6.

[20] A. Shahzad and R. Liu, "Kuhn-tucker conditions for nuclear norm optimization methods for interference alignment," in *Computing, Communications and Applications Conference*, 2012, pp. 24–29.

[21] L. Auria and R. A. Moro, "Support Vector Machines (SVM) as a technique for solvency analysis," *SSRN Electronic Journal*, vol. 1, 2008.

[22] N. Cristianini and J. Shawe-Taylor, "An introduction to support vector machines: And other kernel-based learning methods," *Cambridge University Press*, 2000.

[23] K. S. Ni and T. Q. Nguyen, "Image superresolution using support vector regression," *IEEE Transactions on Image Processing*, vol. 16, no. 6, pp. 1596–1610, 2007.

[24] R. A. Games, D. Moulin, S. D. O'Neil, and J. J. Rushanan, "Algebraic-integer quantization an residue number system processing," in *International Conference on Acoustics, Speech, and Signal Processing*, 1989, pp. 948–951.

[25] L. Wang, Y. Zhang, and J. Feng, "On the Euclidean distance of images," *IEEE Transactions on Pattern Analysis and Machine Intelligence*, vol. 27, no. 8, pp. 1334–1339, 2005.

[26] M. Lindenbaum, "On the amount of data required for reliable recognition," in *Proceedings of 12th International Conference on Pattern Recognition*, vol. 1, 1994, pp. 726–729.

[27] M. Yang, D. Kriegman, and N. Ahuja, "Detecting faces in images: A survey," *Pattern Analysis and Machine Intelligence, IEEE Transactions on*, vol. 24, pp. 34–58, 2002.

[28] C. Gronwall, F. Gustafsson, and M. Millnert, "Ground target recognition using rectangle estimation," *IEEE Transactions on Image Processing*, vol. 15, no. 11, pp. 3400–3408, 2006.

[29] P. Ayyalasomayajula, S. Grassi, and P. Farine, "Rotation, scale and translation invariant image retrieval method based on circular segmentation and color density," in *International Symposium on Image and Signal Processing and Analysis*, 2011, pp. 455–459.

[30] A. Makadia and K. Daniilidis, "Rotation recovery from spherical images without correspondences," *IEEE Transactions on Pattern Analysis and Machine Intelligence*, vol. 28, no. 7, pp. 1170–1175, 2006.

[31] P. Ahmadvand, R. Ebrahimpour, and P. Ahmadvand, "How popular CNNs perform in real applications of face recognition," in *Telecommunications Forum*, 2016, pp. 1–4.

[32] G. Karthick and R. Harikumar, "Comparative performance analysis of naive bayes and svm classifier for oral x-ray images," in *International Conference on Electronics and Communication Systems*, 2017, pp. 88–92.

[33] S. Bernard, L. Heutte, and S. Adam, "On the selection of decision trees in random forests," in *International Joint Conference on Neural Networks*, 2009, pp. 302–307.

[34] S. Zhang, T. Chen, Y. Zhang, S. Hu, and R. R. Martin, "Vectorizing cartoon animations," *IEEE Transactions on Visualization and Computer Graphics*, vol. 15, no. 4, pp. 618–629, 2009.

[35] D. Liu, J. Chen, G. Wu, and H. Duan, "Svm-based remote sensing image classification and monitoring of lijiang chenghai," in *International Conference on Remote Sensing, Environment and Transportation Engineering*, vol. 2, 2012, pp. 1–4.

[36] C. Uriel Paredes-Hernndez, W. Enrique Salinas-Castillo, F. Guevara-Cortina, and X. Martnez-Becerra, "Horizontal positional accuracy of google earth's imagery over rural areas: A study case in tamaulipas, mexico," *Boletim de Ciłncias Geodsicas*, vol. 19, pp. 588–601, 12 2013.

[37] J. L. Kafka and M. A. Miller, "A climatology of solar irradiance and its controls across the United States: Implications for solar panel orientation," *Renewable Energy*, vol. 135, pp. 897 – 907, 2019.

[38] D. P. Bertsekas, *Dynamic programming and optimal control*. Athena scientific Belmont, MA, 2005, vol. 1, no. 3.

[39] V. Mnih, K. Kavukcuoglu, D. Silver, A. Graves, I. Antonoglou, D. Wierstra, and M. Riedmiller, "Playing atari with deep reinforcement learning," *arXiv preprint arXiv:1312.5602*, 2013.